Thermal X-ray radiation from hot polar cap in pulsars with drifting subpulses

Janusz Gil

J. Kepler Astronomical Institute
University of Zielona Góra,
Poland

Collaborators:

G. Melikidze, B. Zhang, U. Geppert, F. Haberl

40 years after discovery of pulsars the actual mechanism of their coherent radio emission is still a mystery.

Drifting subpulses, which seem to be a common phenomenon in pulsar radiation, is also a puzzle.

„The mechanism for drifting subpulses cannot be very different from the mechanism of observed radio emission ...

...intrinsic property of radiation mechanism „

(Weltevrede, Edwards & Stappers 2006, A&A 445,243)

Unbiased search for drifting subpulses in 187 (191) pulsars

About 55 % (more) of drifting subpulse pulsars

Weltevrede, Edwards & Stappers et al. 2006, 2007

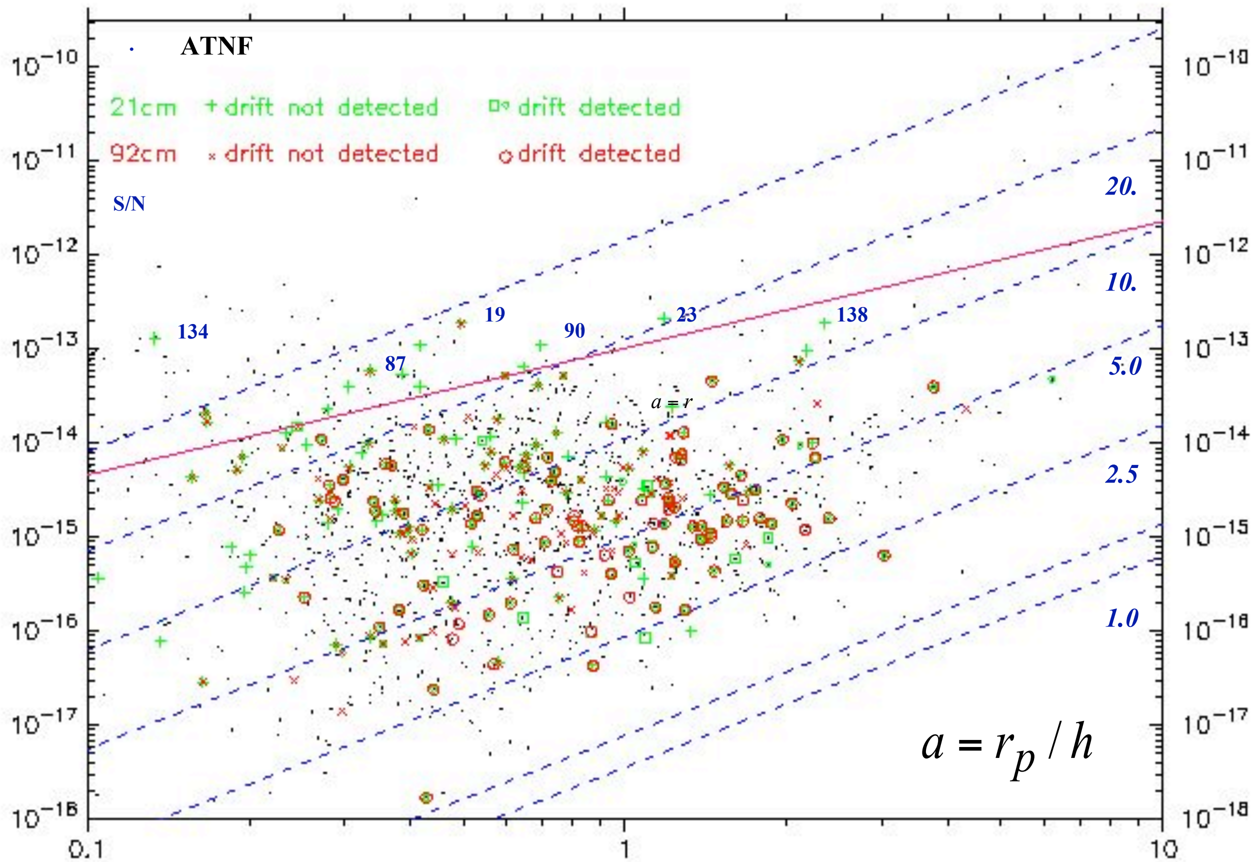

At frequencies lower than 320 MHz (LOFAR range) the ratio of detected drifting subpulses should be even higher

Assumptions and background

1. Unballanced charge depletion causes huge potential drop above PC
   a. this requires strong binding of surface components
   b. which in turn requires very strong (above 10^13 – 10^14 G) nondipolar surface magnetic field (for all pulsars)

2. The potential drop is limited by the magnetic electron-positron pair production, which terminates the plasma outflow at some „gap" height *h~5 – 50 meters*
   a. this requires strong and curved magnetic field at the PC surface
   b. which is authomatically fullfilled if the surface field is highly non-dipolar

   Electrons are falling back and heat the PC surface, while positrons flow out of the acceleration region to take part in the radio emission generation process.

3. The pair production is non-stationary and localized. It takes a form of isolated sparks that tend to populate the PC surface as densely as possible. Each spark discharges the space around itself to within a distance of about gap height *d~h.* This is also a charakteristic dimenssion of each spark *D~h.*

4. Each spark developes until the pair production screens completely the voltage above the PC (this takes about few microseconds). The foot of a spark is heated to few MK by the back-flow of electrons accelerated towards PC.

5. After the spark is quenched its foot is still hot and have a small cloud of thermal electrons above it. When the spark plasma empties the gap region, the returning potential drop accelerates thermal electrons and innitiates the very next spark in the same place.

Polar cap radius and bolometric surface area

Locus of the open magnetic field lines

$$r_p = 1.45 \times 10^4 P^{-0.5}\ cm$$

Canonical radius for dipolar field lines at the NS surface

$$r_{pc} = b^{-0.5} r_p$$

Actual value for non-dipolar surface field

$$b = B_s / B_d = A_p / A_{pc} = A_p / A_{bol}$$

B_s **Actual field**

B_d **Dipolar field**

$$A_p = \pi r_p^2$$

canonical

Surface area

bolometric

$$A_{pc} = \pi r_{pc}^2 = b^{-1} A_p$$

Bolometric area should be much smaller than the canonical one !
In many cases the hot spot is really smaller than the conventional PC, but there are few cases with larger surface area than that of PC.

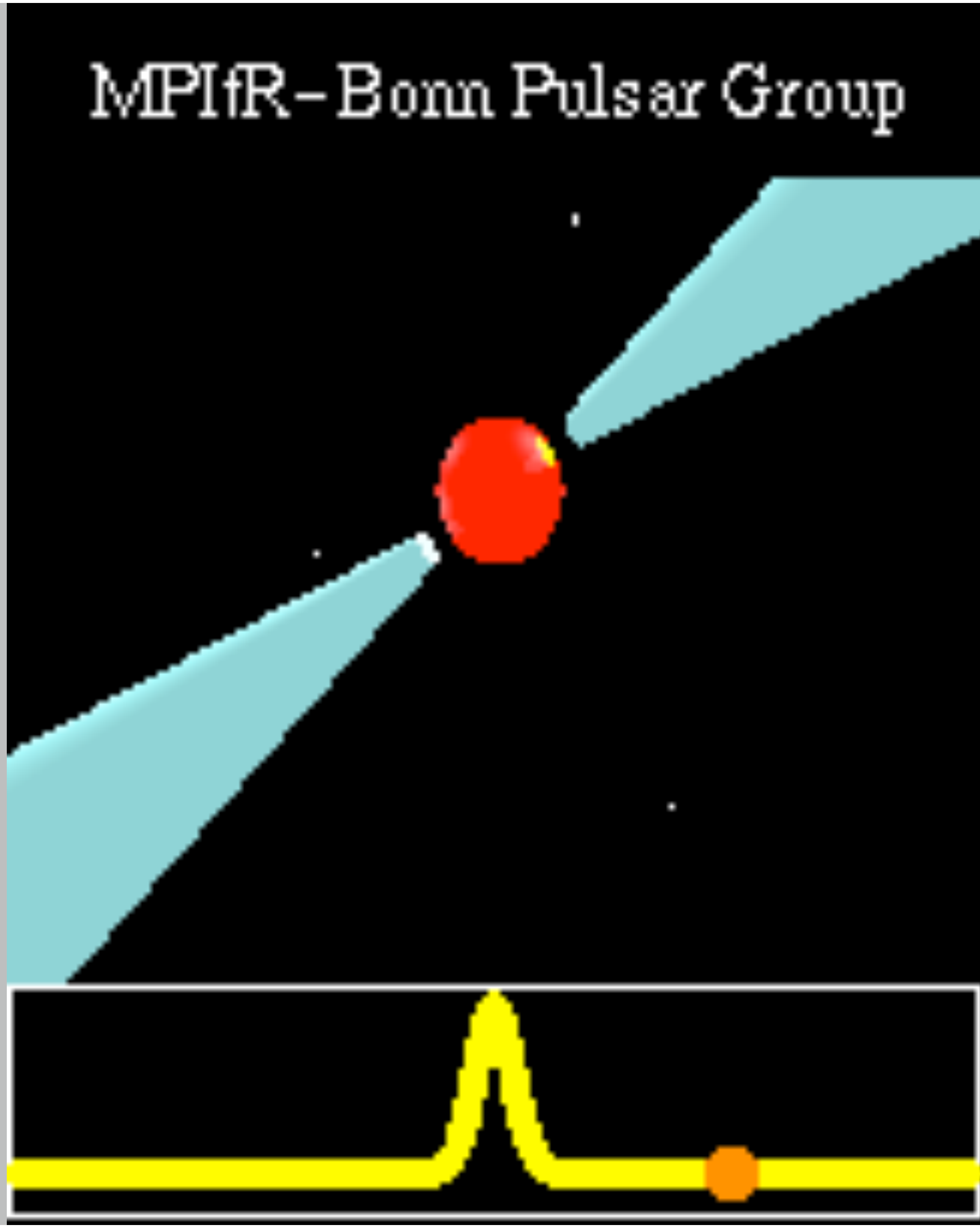
MPIfR - Bonn Pulsar Group

Carousel model

Sub-beams of radio emission presumably related to sparks operating just above the Polar Cap circulate around the magnetic axis

Subpulse drift

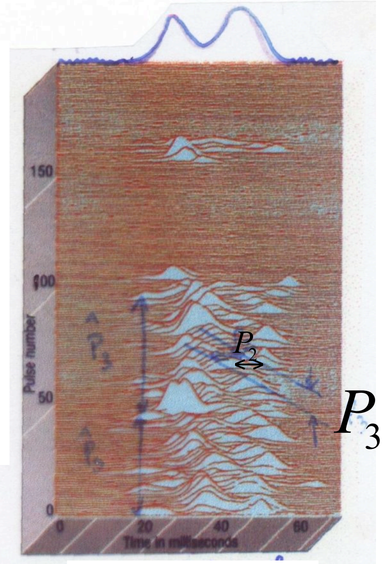

Subpulses in subsequent pulses arrive in phases determined by the apparent drift rate

P_3 $\quad D = P_2 / P_3$

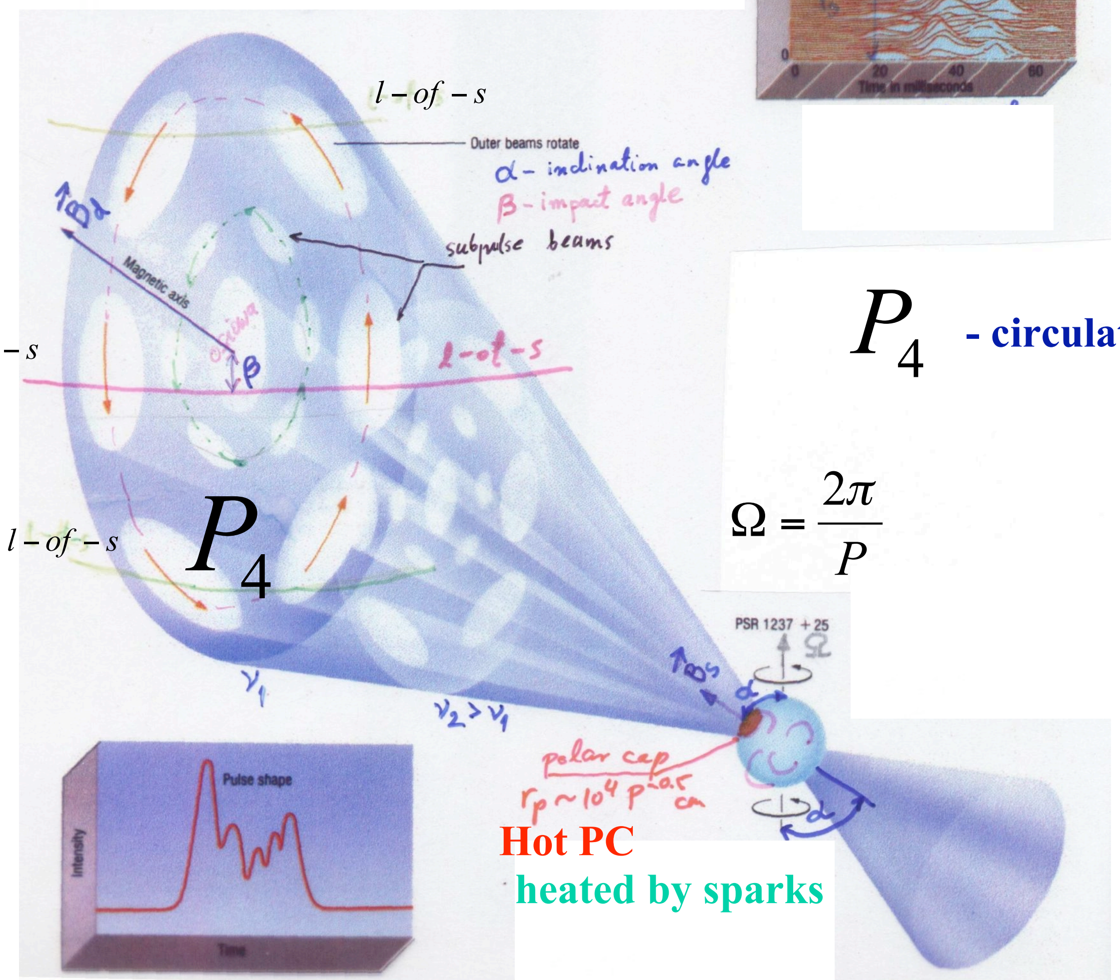

P_4 **- circulational periodicity ?**

$$\Omega = \frac{2\pi}{P}$$

Hot PC
heated by sparks

Polar cap

$$r_{pc} = 1.45 \times 10^4 P^{-0.5}\, cm$$

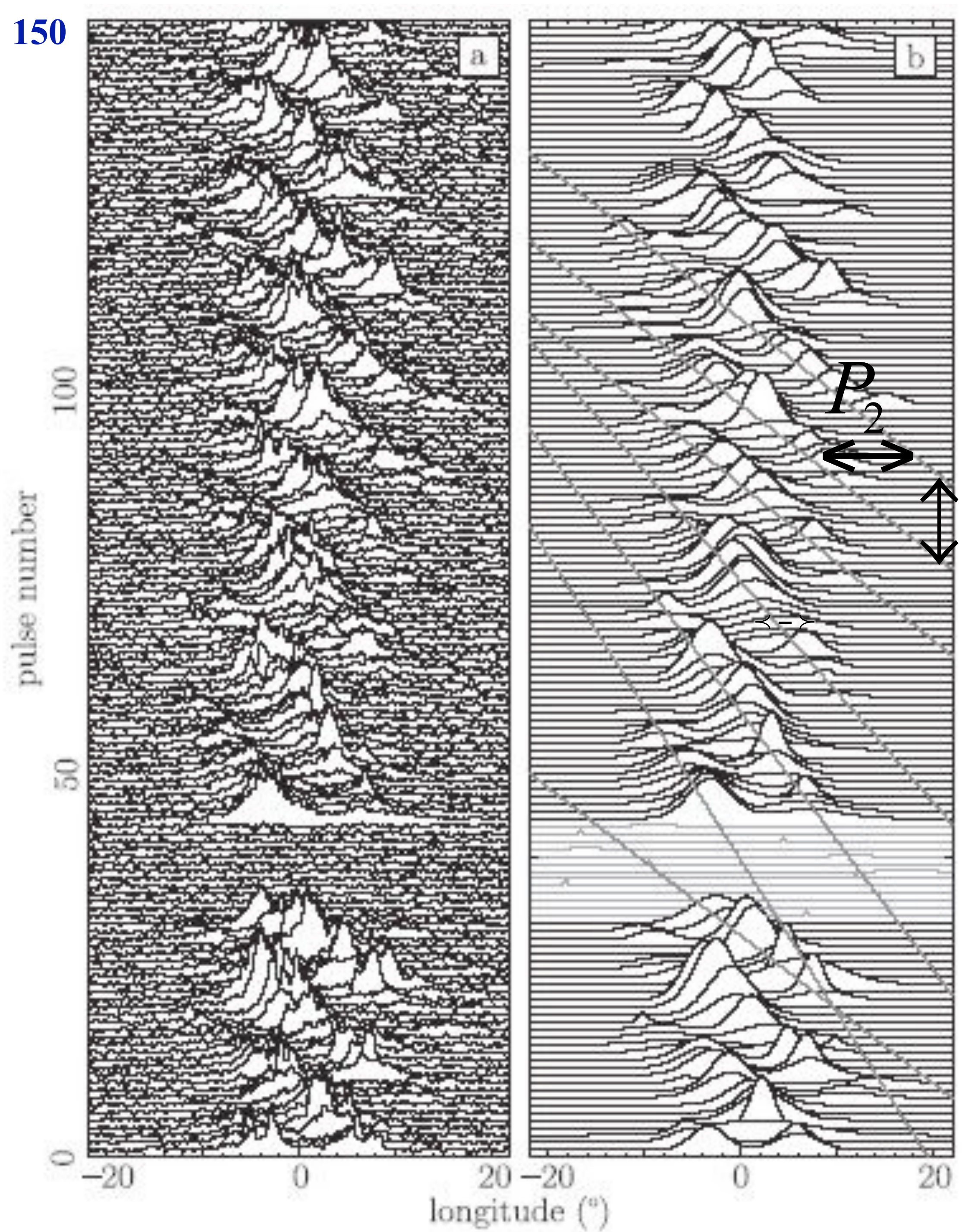

PSR B0809+74

Line-of-sight (l-of-s) grazing the overall pulsar beam

Apparent subpulse drift-bands

$P_3 \approx 11P$

Modulation of intensity along drift-bands consistent with carousel model

that is

Sub-beams seem to continue to circulate beyond the observed pulse-window

(after van Leuven, Stappers et al..)

PSR B0818-41 Bhatacharya, Gupta, Gil (2007) MNRAS, 377, L10

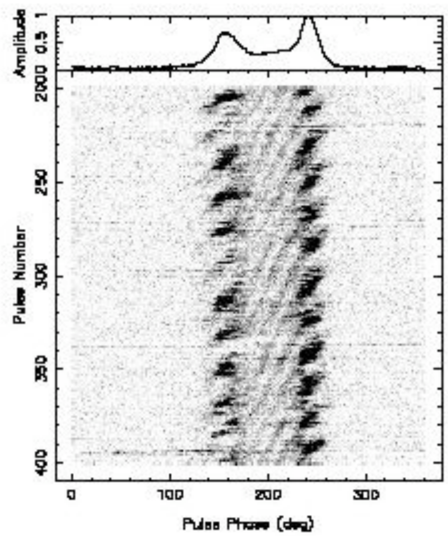

Figure 2. Grey-scale plot of single-pulse data (pulse # 200 to 400) of PSR B0818−41 at 325 MHz, with the average profile shown on top. Signatures of radio frequency interference are present around pulse numbers 220, 298, 338 and 397.

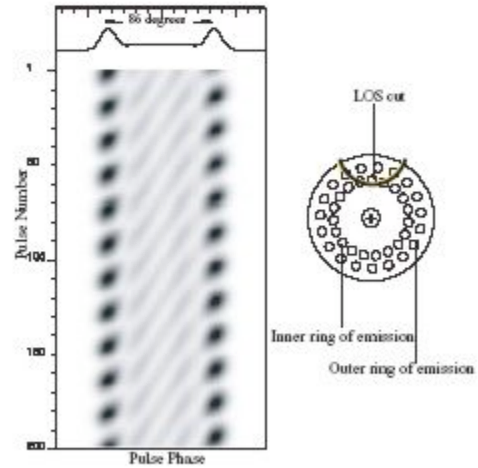

Figure 7. Simulation of the subpulse drift pattern with simple dipolar geometry for the case: $\alpha = 11^\circ$, $\beta = -5\overset{\circ}{.}4$; drift rate = $20^\circ/P_1$.

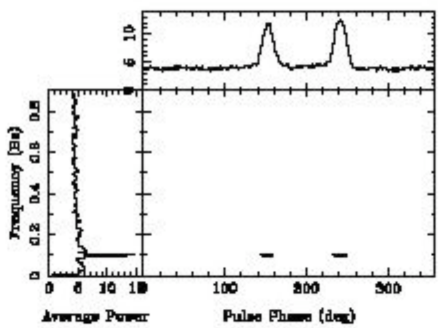

Figure 4. The contour plot of the power spectrum of the flux as a function of pulse phase during a sequence of 200 pulses (pulse # 200–400). The left-hand panel shows the power spectrum integrated over the entire pulse longitude. The upper panel shows the power integrated over fluctuation frequency.

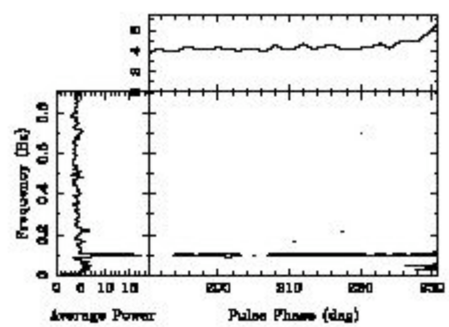

Figure 5. Same as Fig. 4, but for the inner drift region only.

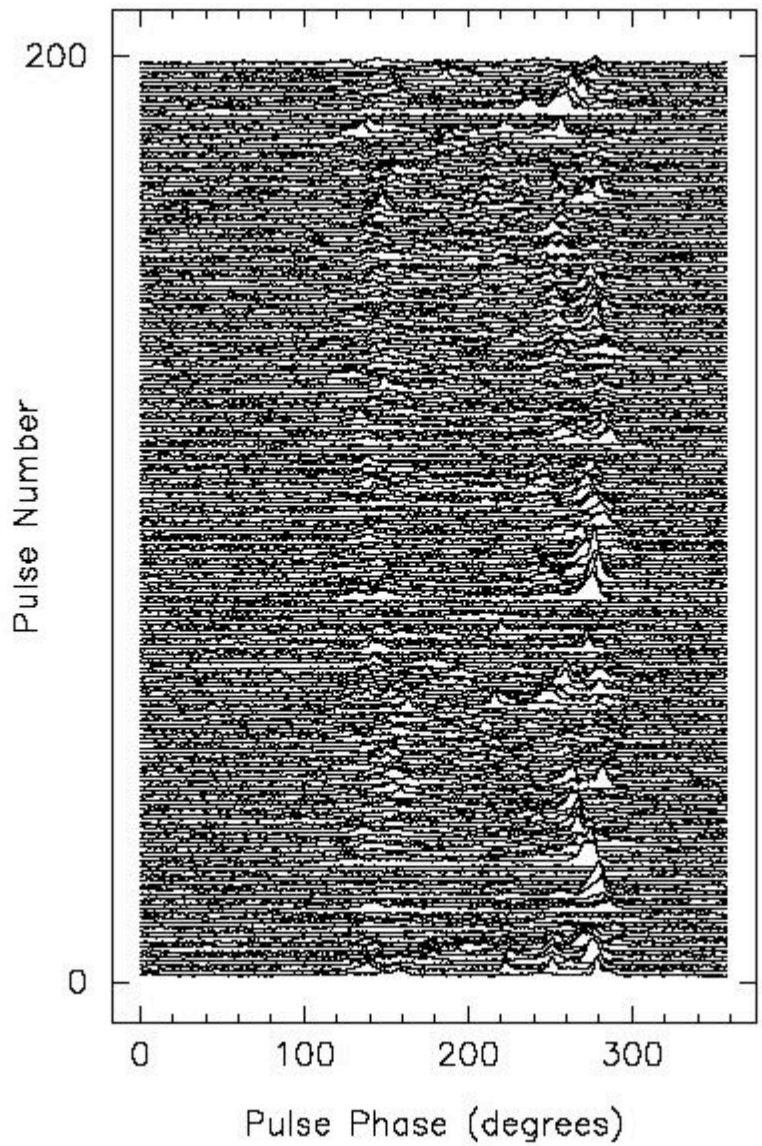

Gupta, Gil et al. 2004

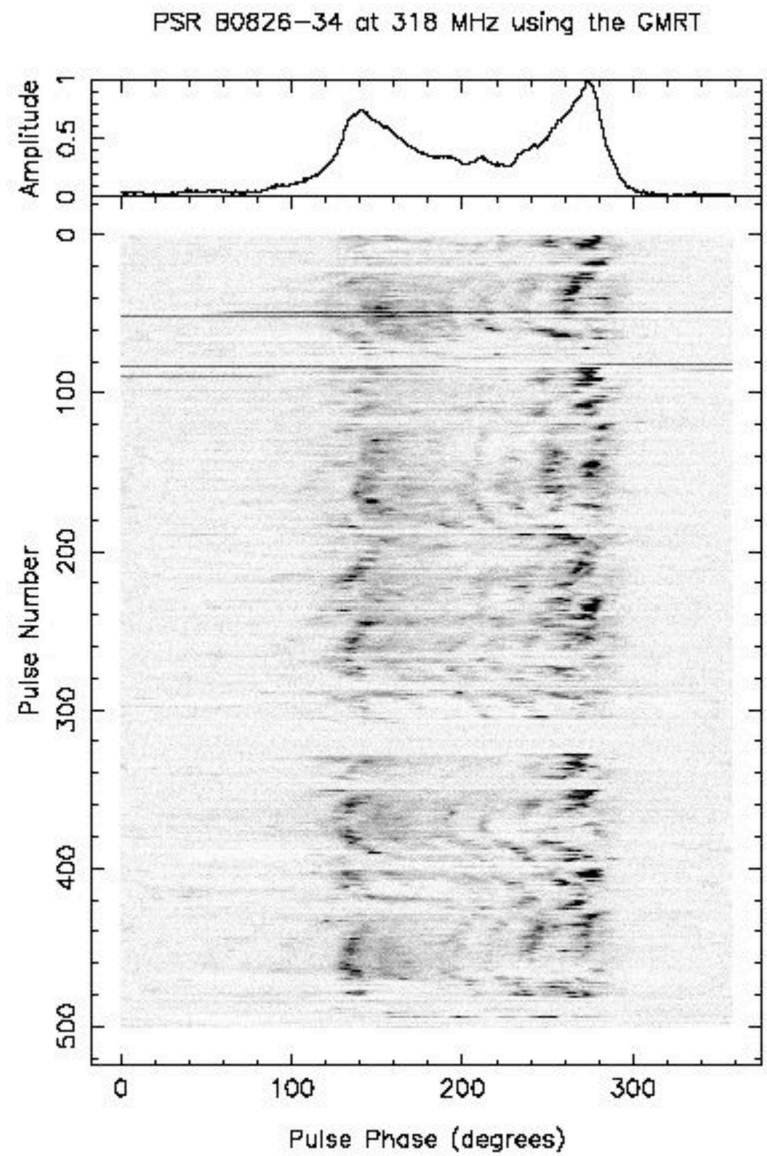

Almost aligned rotator

on Media Help

PSR B0826-34 P_4=14 P Gupta, Gil et al.. 2004

Single pulse analysis results at 1060 MHz

- Main pulse region :

  5–6 drift bands

  (now getting fainter).

- Interpulse region :

  3–4 drift bands

  (much brighter)

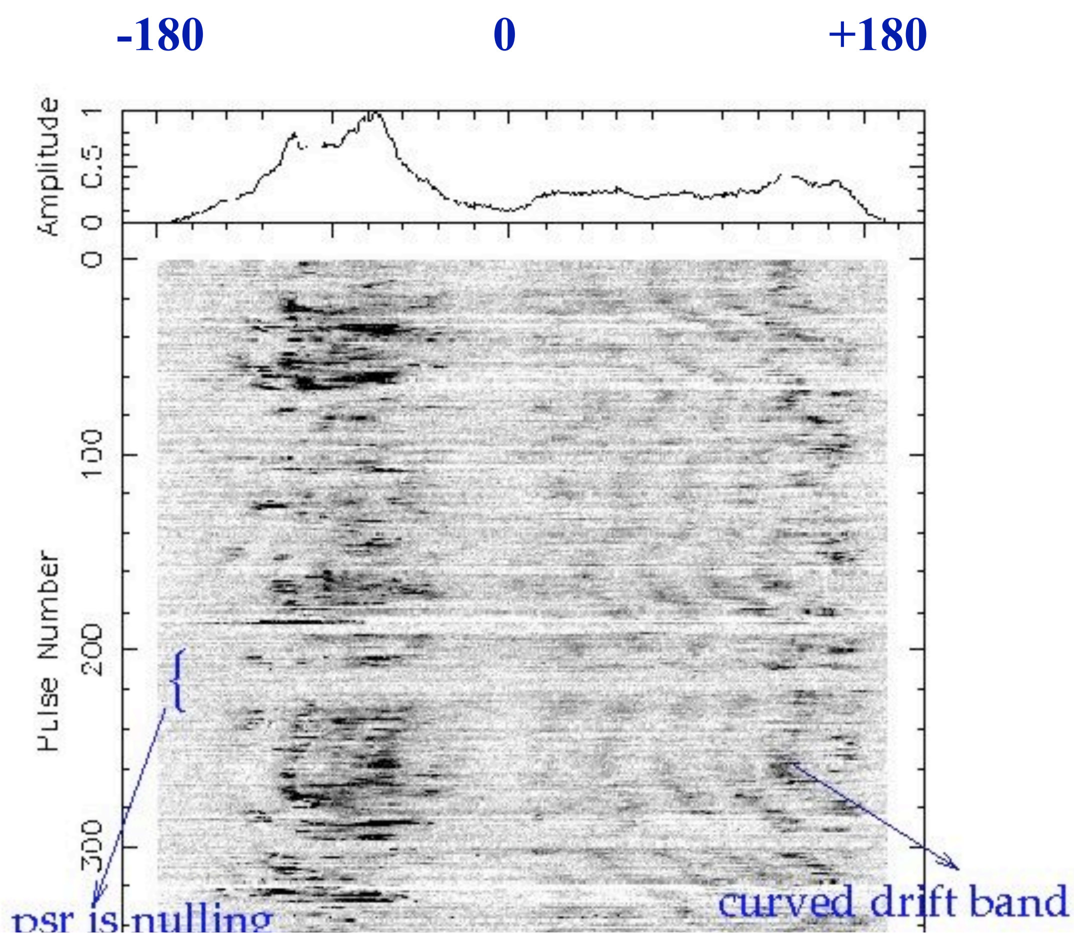

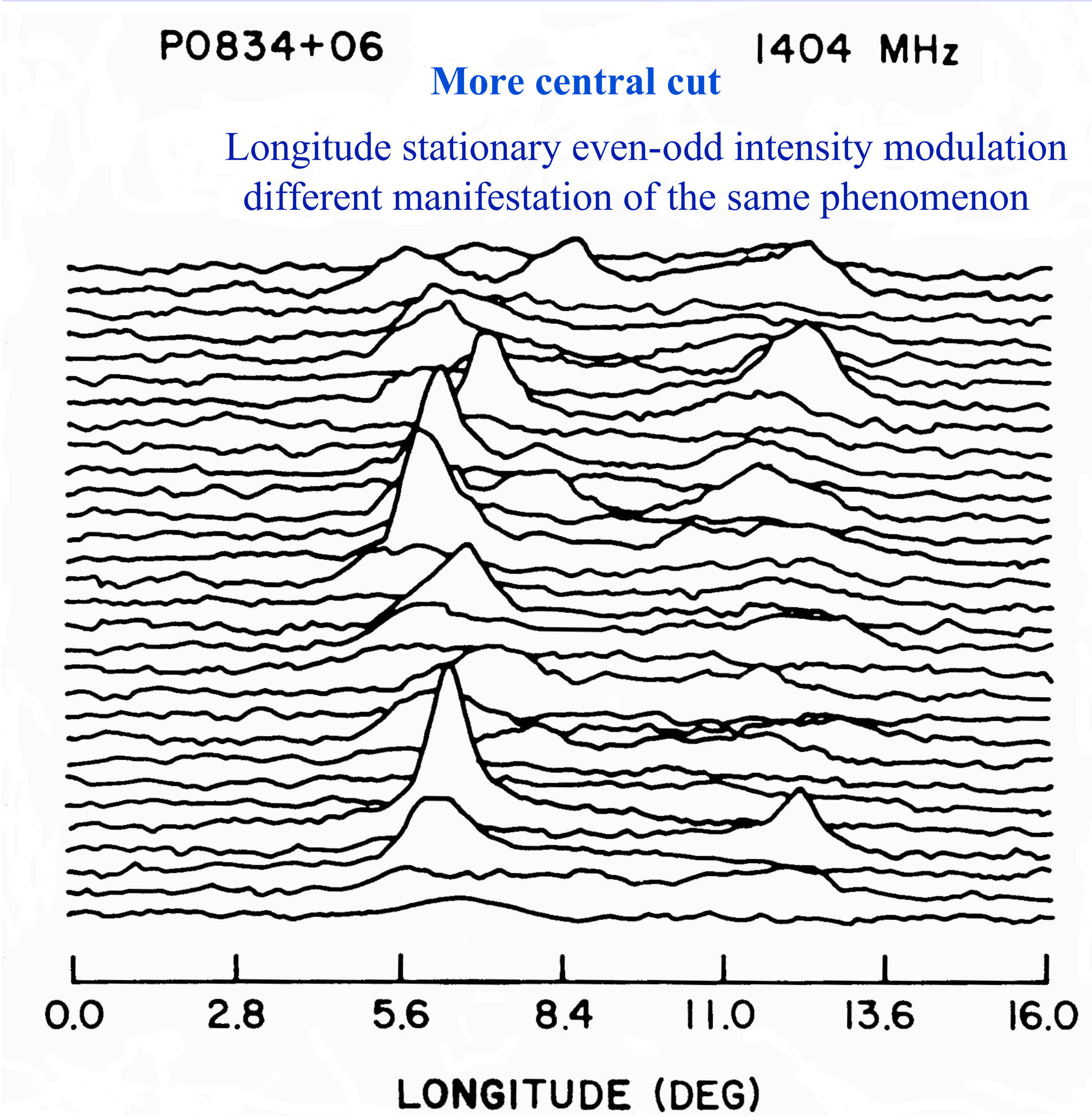

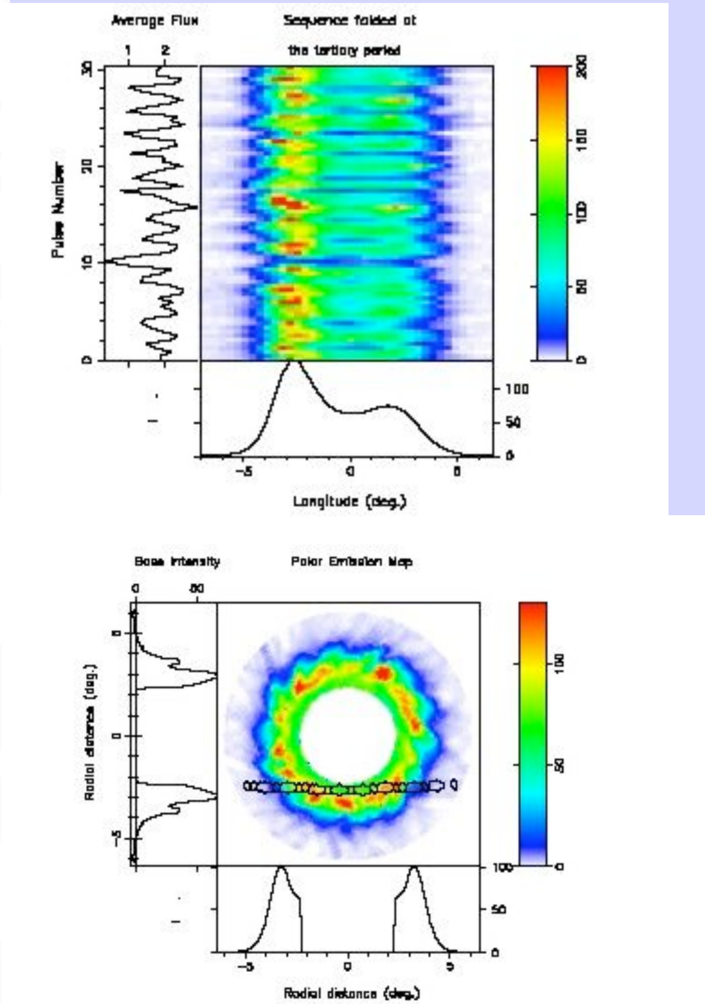

Rankin et al. 2007

Gil & Hankins (1976)

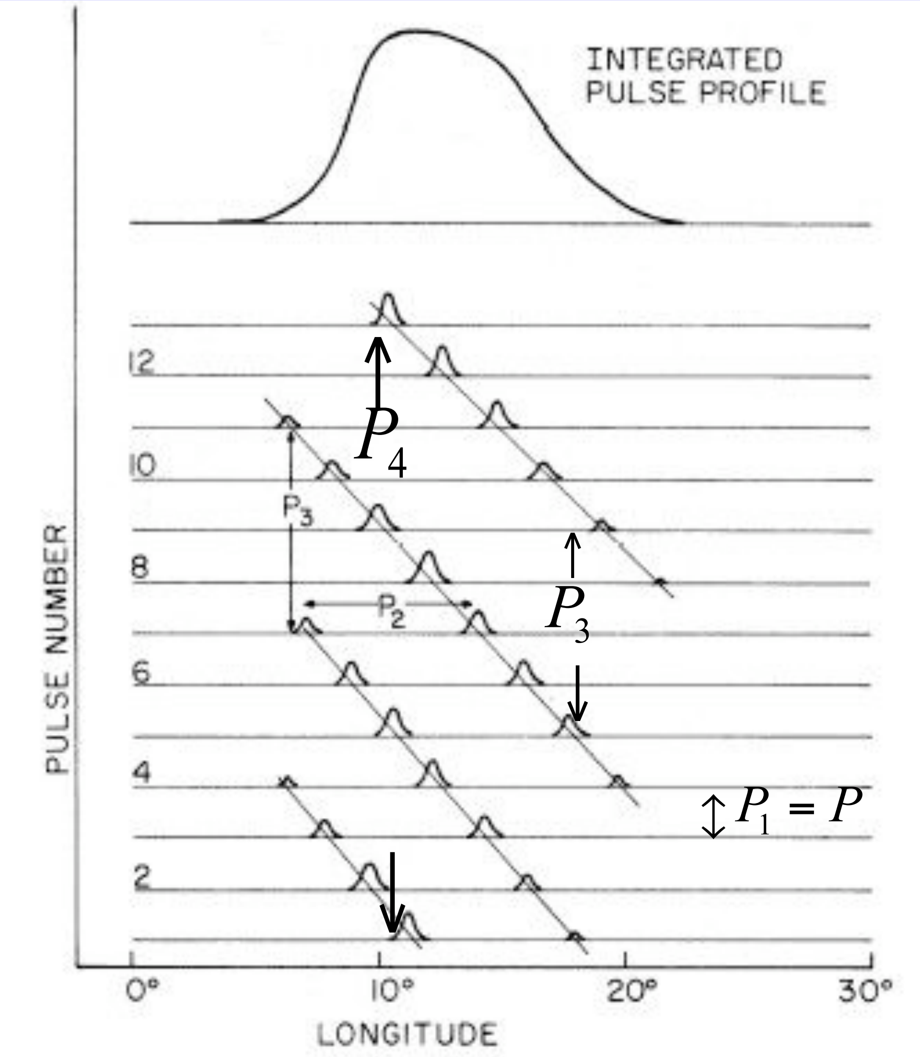

FIG. 5.—Schematic (after Backer 1973) of integrated pulse profile, arrival times of individual pulses, and definition of P_2, P_3 for those pulsars showing the "drifting subpulse" phenomenon. Arrival times of individual pulses are given in terms of a longitude for which 360° corresponds to the full pulsar period.

Ruderman & Sutherland 1975

$$P_1, P_2, P_3, P_4$$

Apparent drift rate $D = P_2 / P_3$

P_2 **distance between driftbands in longitude**

P_3 **distance between driftbands in** P_1

Intrinsic drift rate $P_4 = P_3 N$

N **number of rotating sub-beams**

P_4 **distance between the same driftbands**

P_4 **time interval to complete one rotation around the pole**

very difficult to measure, only 8 cases known !!!

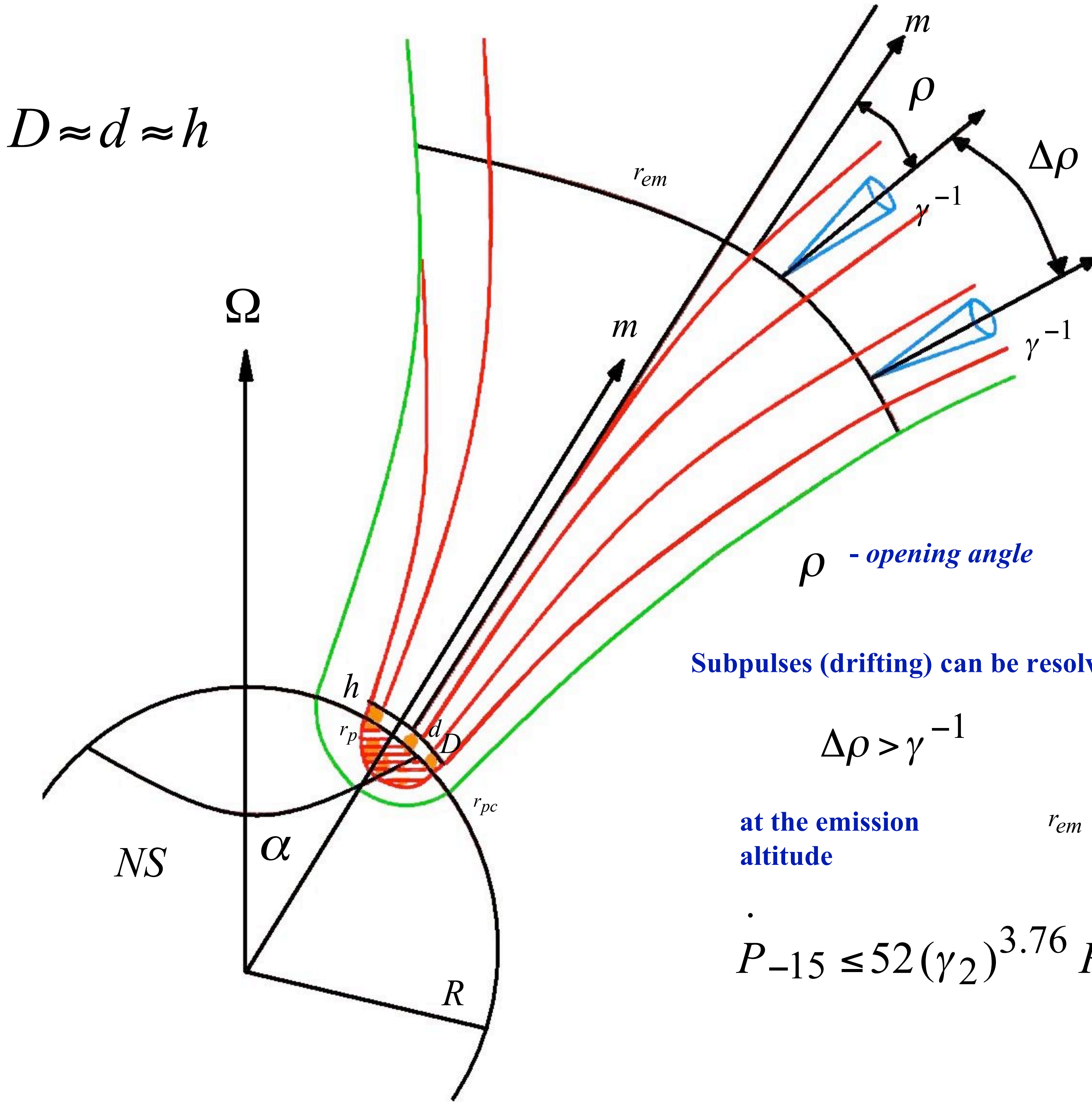

Subpulses (drifting) can be resolved if

$$\Delta\rho > \gamma^{-1}$$

at the emission altitude r_{em}

$$\dot{P}_{-15} \leq 52(\gamma_2)^{3.76} P^{1.35}$$

Unbiased search for drifting subpulses in 187 (191) pulsars

About 55 % (more) of drifting subpulse pulsars

Weltevrede et al. 2006, 2007

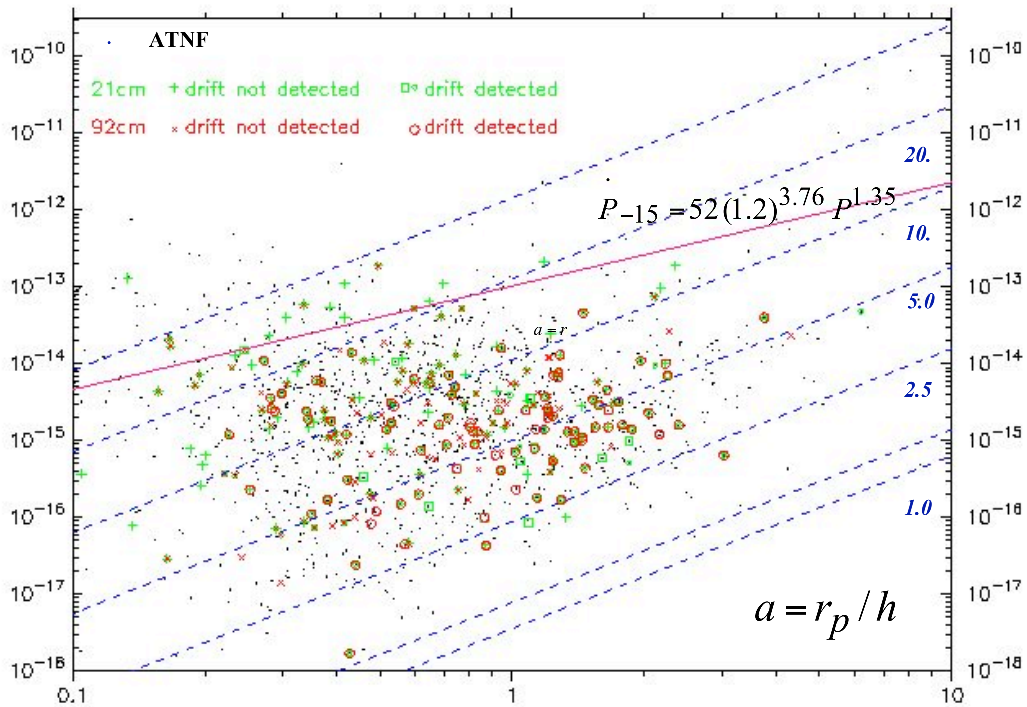

Lorentz factor

$$\gamma = 120$$

Drifting subpulses could really represent subbeams of $1/\gamma$ angular extent , rotating slowly around the magnetic axis

PSR B0943+10

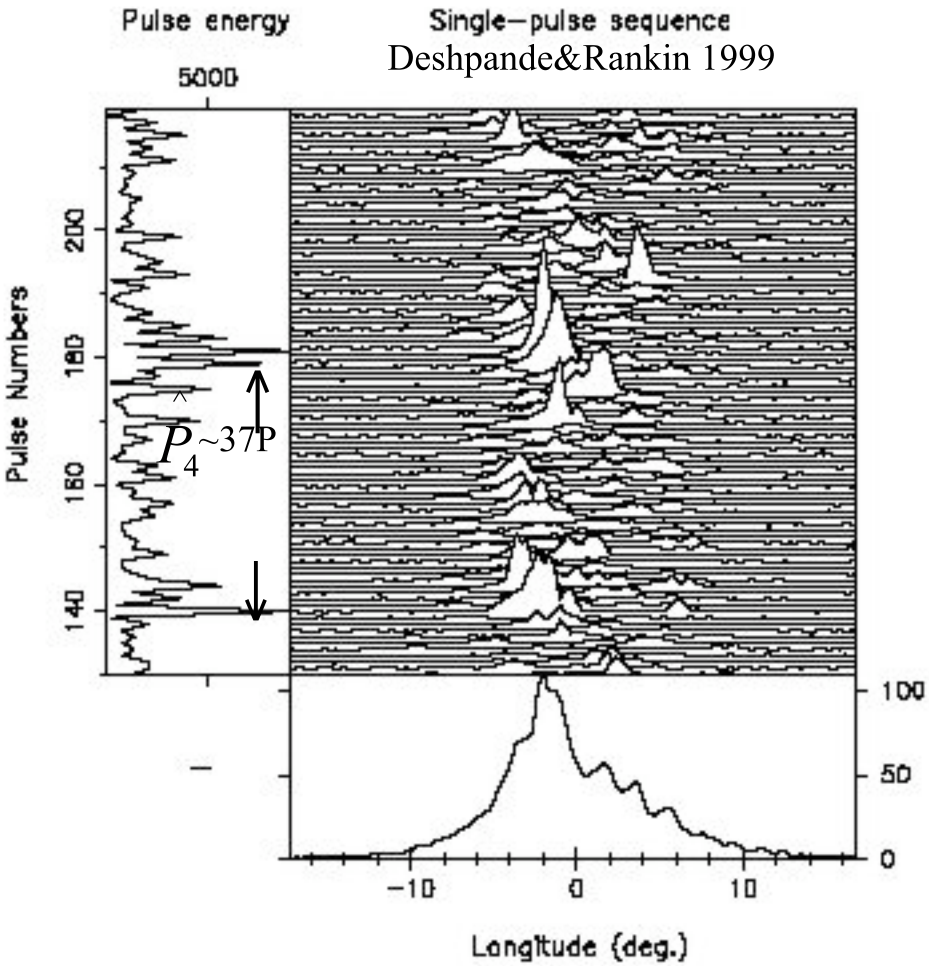

P=1.089 s

$P_3 = 1.87P$ primary

$P_3^{'} = 2.15P$ aliased

$P_4 = 37.35P$

Number of sub-beams circulating around B

$N = P_4 / P_3 = 20$

PSR B0943+10

Deshpande & Rankin 1999, 2001
Asgekar & Deshpande 2001

Phased-resolved fluctuation spectrum

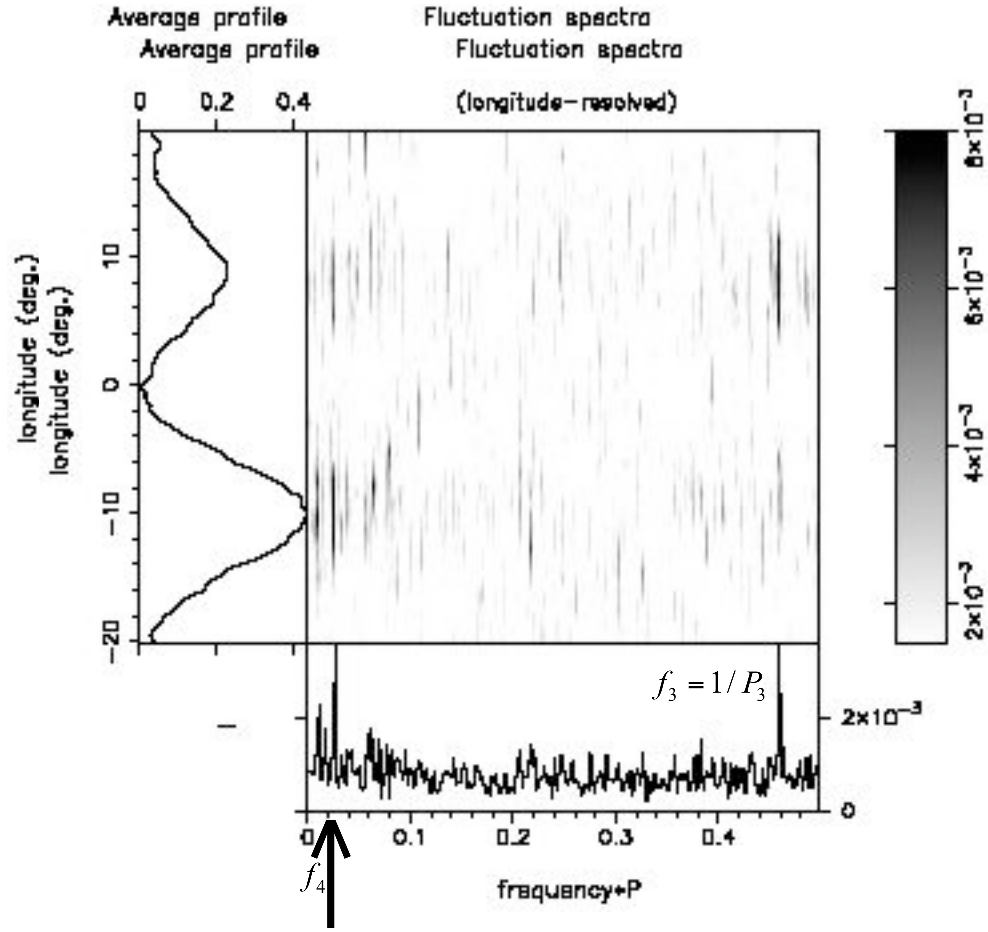

1/37=0.027

$$P_4 = 37.35\,P = 41\text{s.}$$

$$N = P_4 / P_3 = \frac{37.35}{1.87} = 20$$

Spectral analysis fully consistent with „carousel model". Sub-beams continue to circulate around the beam axis beyond the pulse-window and reapear after the period needed to complete one full circulation around the magnetic axis

20 sub-beams

B0943+10 Cartographic map of 20 subpulse beams „circulating” around the pole in about 37 pulsar periods
Deshpande & Rankin, 1999

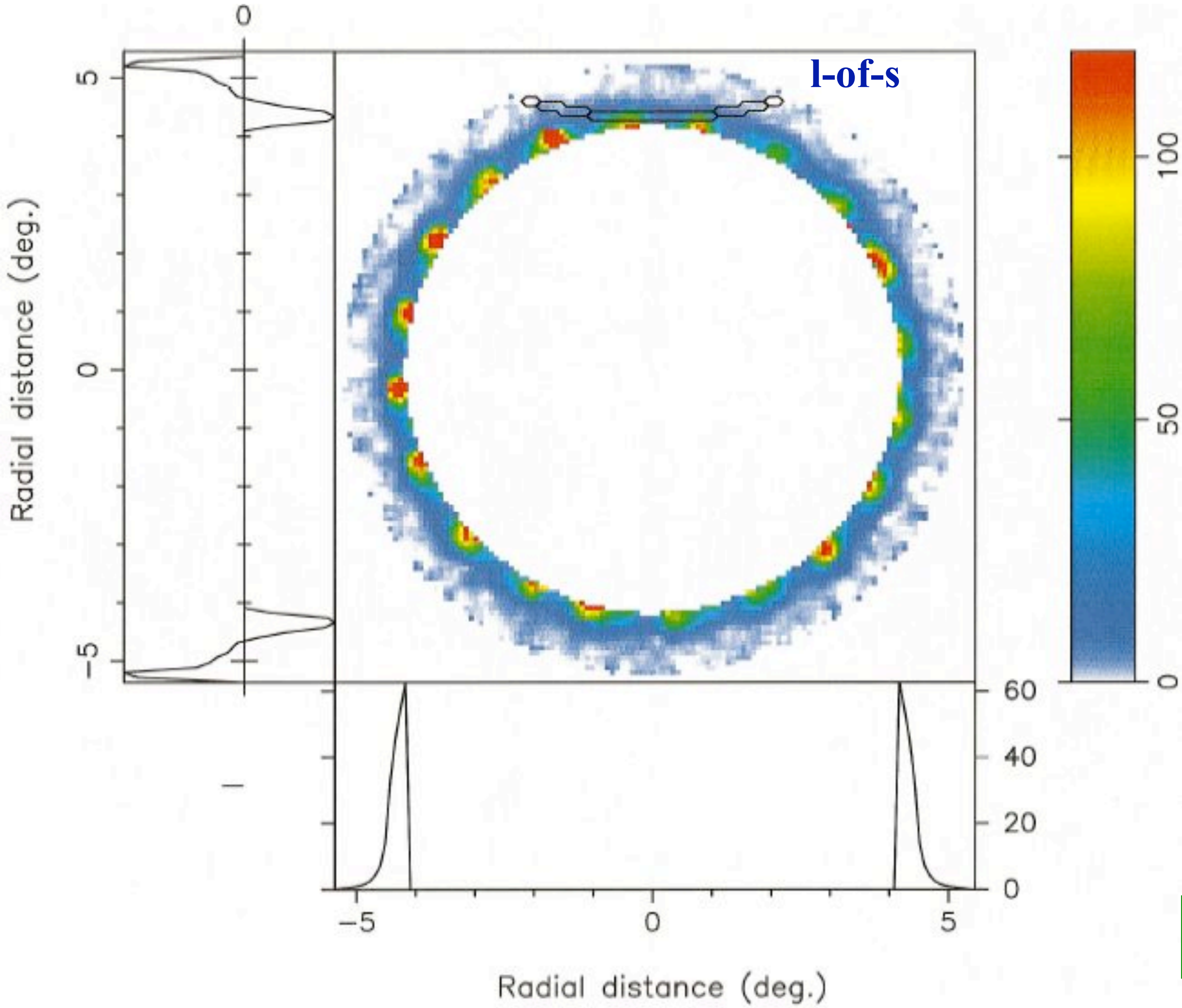

$P = 1.098$ s

$P_3 = 1.86\ P$

$P_4 = 37.35\,P$

$N = P_4 / P_3 = 20$

α, β *Pulsar geometry known*

(Intensity; pulse longitude and pulse number) →(Intensity; polar colatitude and azimuth)

Clear manifestation of subpulse sub-beams circulating around the magnetic axis

Radius-to-frequency mapping

Frequency dependent beam size

PSR B0943+10

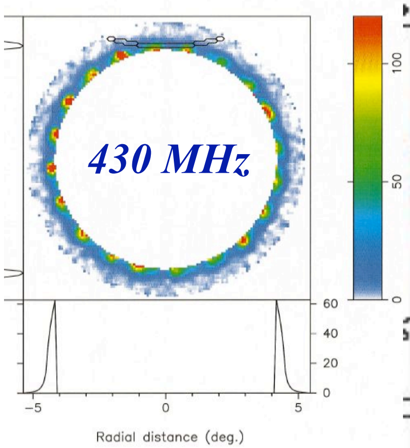

Arecibo

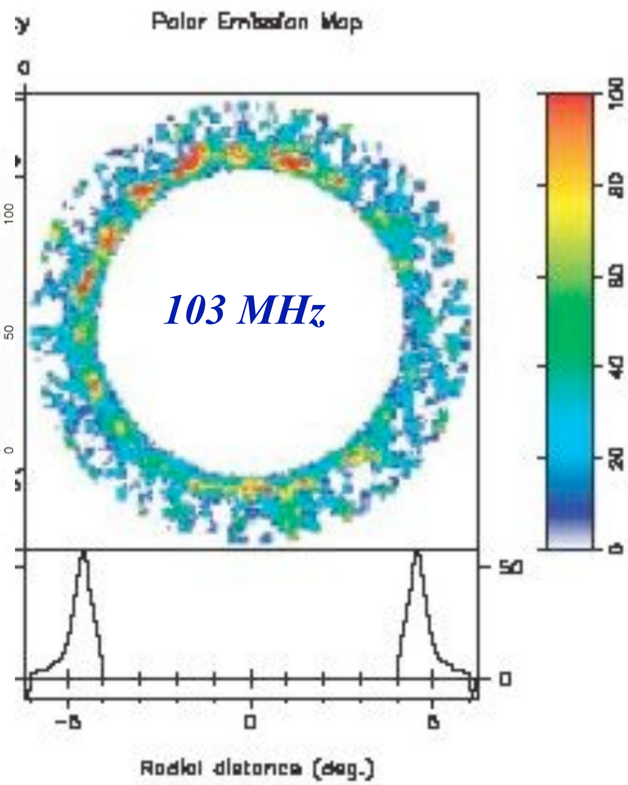

PRAO

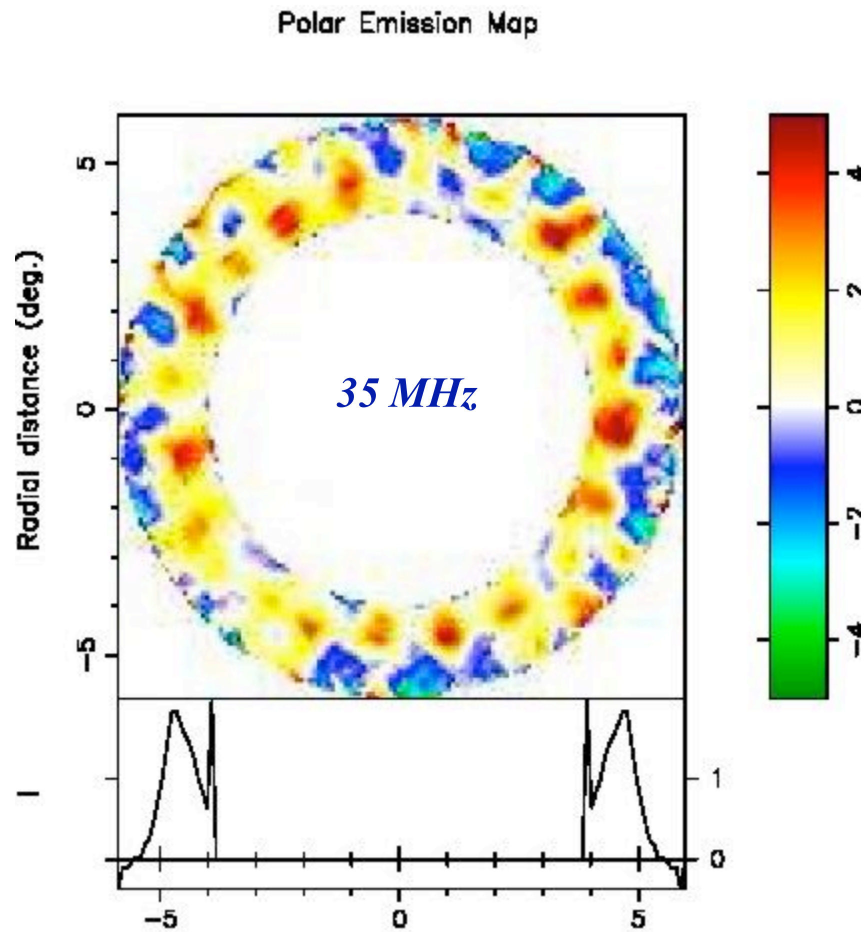

Gauribidanur

Sometimes regular drifters turn into more erratic or even chaotic mode in which regular drift pattern is not visible at all. However, the fluctuation spectrum analysis still reveals a low frequency periodicity, while high frequency feature often dissapears.

B0943+10 430 MHz

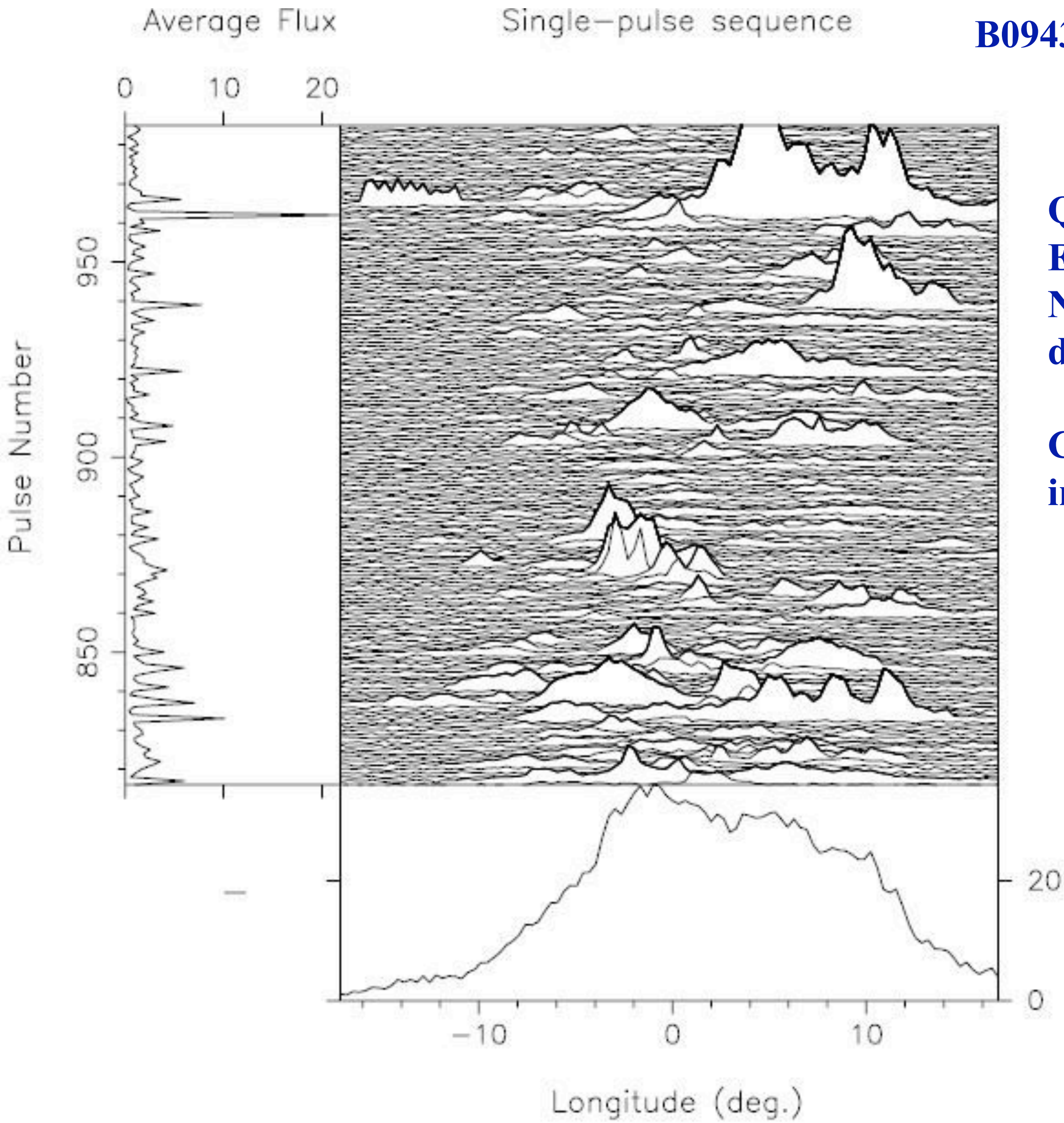

Q-mode
Erratic
No organized drift visible

Cartographic map impossible to make

103 MHz

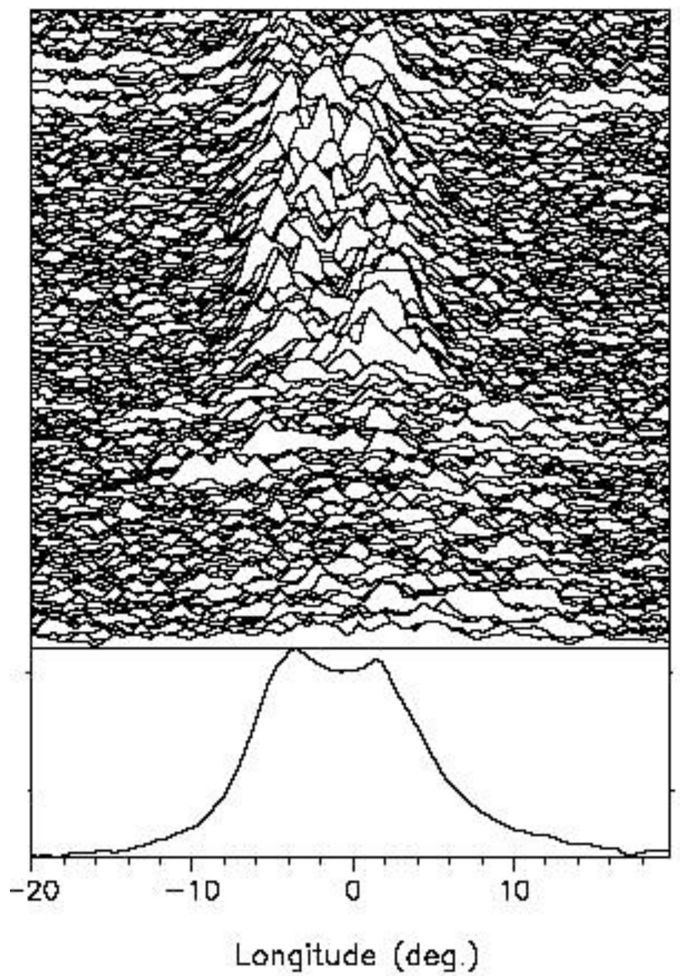

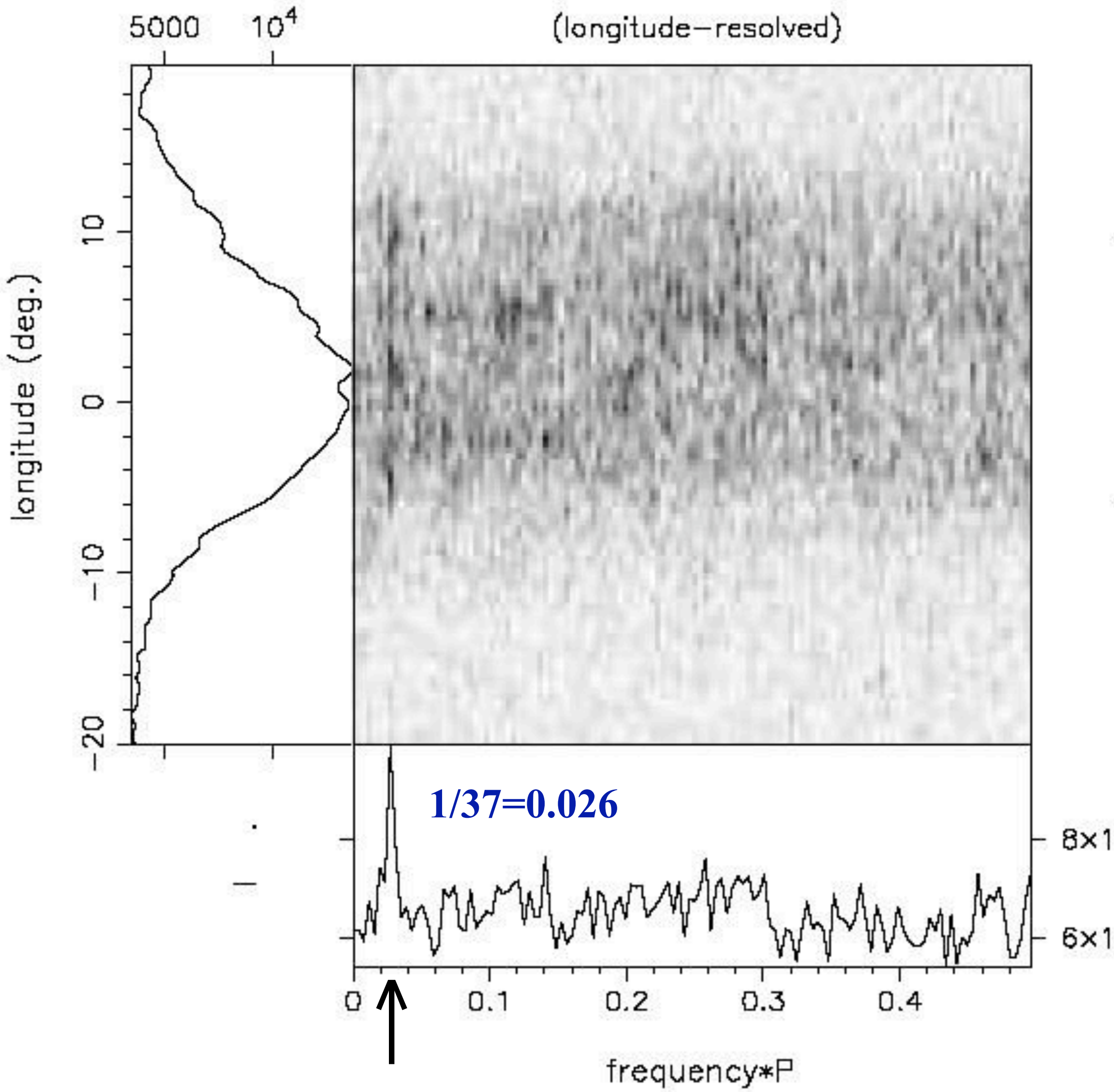

Clear feature at 37 P as in the B-mode

B0943+10 Q-mode (erratic)

Suleymanova & Rankin 2006

Spark plasma circulates around the local magnetic pole on the Polar Cap with a specific period P_4 , regardless it is fragmented into equally spaced filaments or operates in much less organized manner.

Natural mechanism of subpulse drift

$$E \times B$$

Natural state of the magnetospheric plasma frozen into electric and magnetic field is corotation with NS (global corotation)

R & S (1975)

$$\upsilon_{cor} = c(E_c \times B_s)/B^2 = cE_c/B_s \quad \Leftarrow \rho = \rho_{GJ}$$

corotation

$$if \quad E \neq E_c \quad then \quad \upsilon \neq \upsilon_{cor} \quad \Leftarrow \rho \neq \rho_{GJ}$$

Polar Gap charge depletion

Non-corotation plasma lags behind pulsar rotation and drifts with respects the polar cap surface with velocity υ_{dr}

$$\upsilon_{dr} = c(\Delta E \times B_s)/B^2 = c\Delta E / B_s$$

ΔE Electric field associated with charge depletion $\Delta\rho = \rho_{GJ} - \rho$

If plasma has transversal structure (spark filaments) then this inevitable

$\Delta E \times B$ **drift should be observed in the form of drifting subpulses, and/or specific features in the intensity fluctuation spectrum**

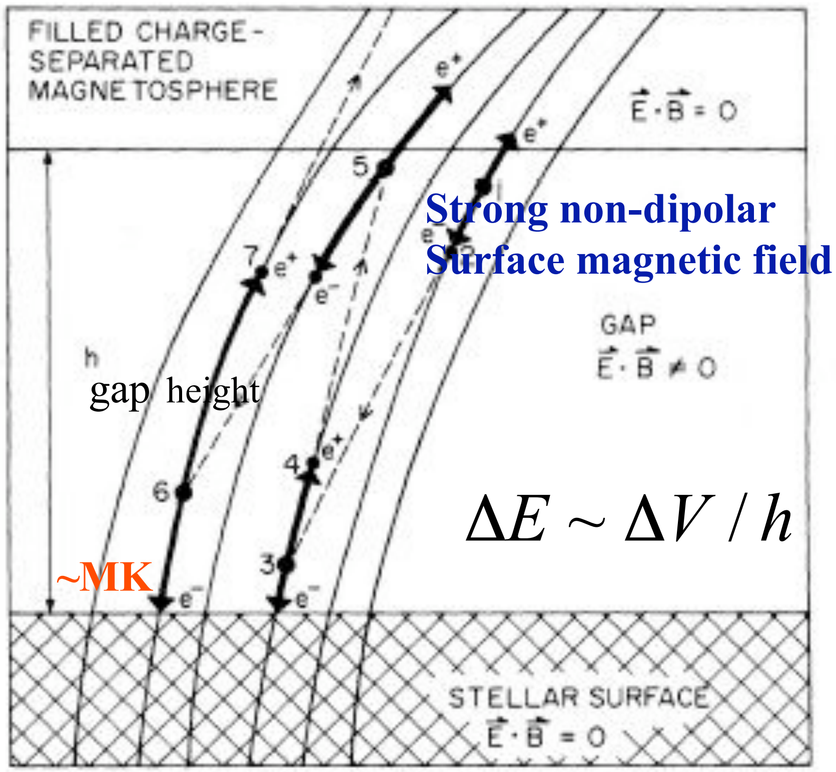

$$\Delta E \sim \Delta V / h$$

Within the acceleration region the spark generated positrons are moving towards the magnetosphere while back-flow of electrons bombard the polar cap surface and heat it to MK temperatures

Ruderman & Sutherland 1975

Pure vacuum gap

Charge depletion maximum possible $\Delta\rho = \rho_{GJ}$

Very strong electric field ΔE

$\Delta E \times B$ **drift much too fast as compared with observations**

Polar cap heating too intense and subpulse drift was too fast as compared with observations

Modification needed

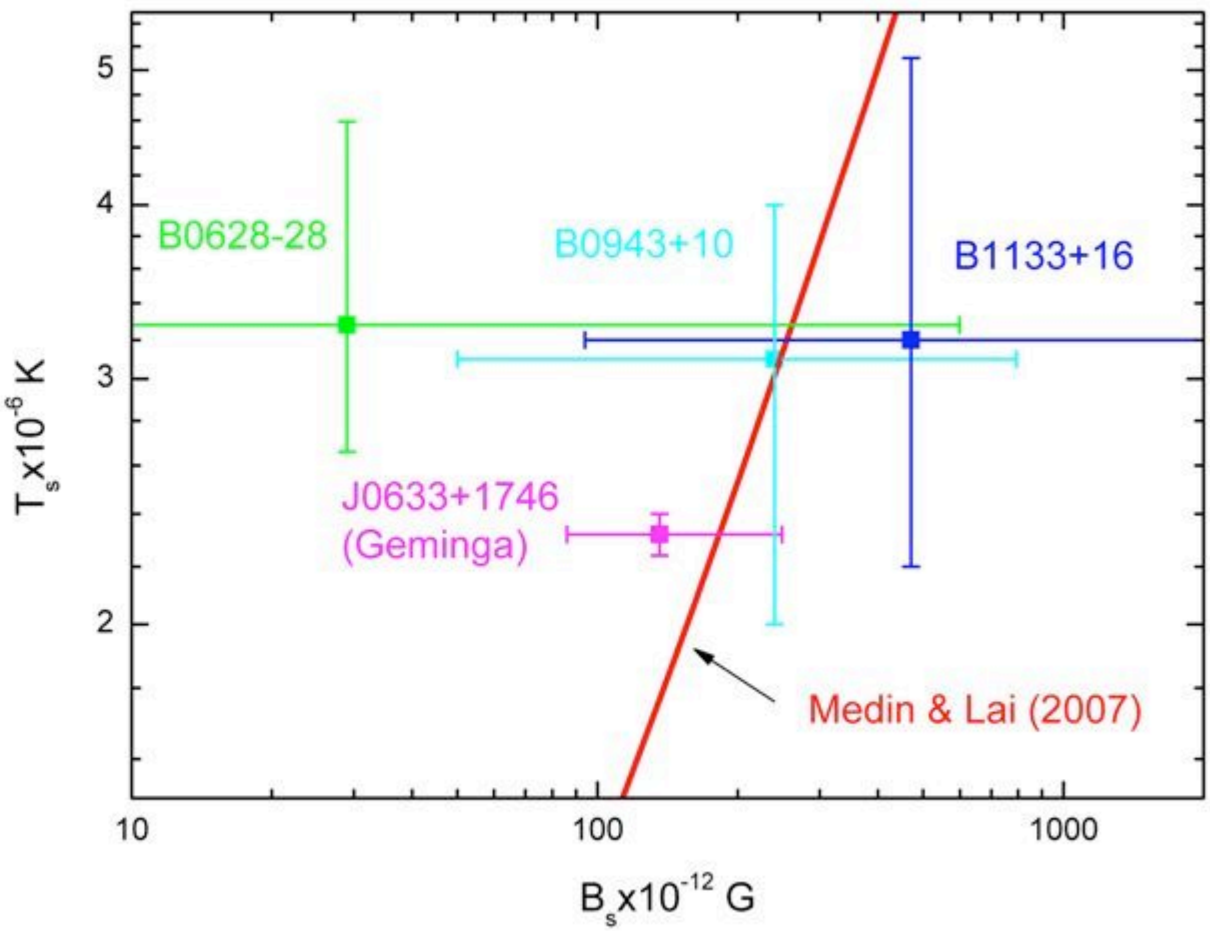

B0628-28
B0943+10
B1133+16
J0633+1746
(Geminga)
Medin & Lai (2007)
5
4
3
2
10
100
1000
T_sx10^{-6} K
B_sx10^{-12} G

Partialy Screened Gap (PSG) model

Gil, Melikidze & Geppert 2003

Electron-positron plasma created in sparks co-exists with thermionic flow caused by back-flow bombardment

$$\rho_{\pm} + \rho_{th} = \rho_{GJ}$$

Surface temperature of spark-heated polar cap

$$T_s \geq 10^6\ K \qquad T_s \leq T_i$$

$$T_i = \varepsilon / 30k = (7 \times 10^4\ K)(B_s / 10^{12}\ G)^{0.7}$$

Ion critical temperature (Jones 1986, Medin & Lai 2006)

$$B_s \sim 10^{13-14}\ G$$

above this T there is maximum thermionic flow from the PC surface with GJ density (no sparking)

$$\eta = 1 - \rho_{th} / \rho_{GJ} = 1 - \exp[30(1 - T_i / T_s)]$$

Screening factor determined by thermoregulation of PSG

Thermoregulation of PSG

Backflowing bombardment associated with spark plasma development heats the PC surface to temperatures lower than critical temperature (above which there is free flow).

The higher the temperature the more intense thermionic emission, which in turn means more screening and less intense heating.

This thermolegulation should establish the quasi-steady state at temperature very close (but slightly lower) to the critical temperature

$$T_s \cong T_i$$

Spark-associated polar cap heating within partially screened gap model

$$L_x = A_{bol}\sigma T_s^{\ 4} = A_{bol}\gamma m_e c n$$

Back-flow bombardment

$$\gamma = e\Delta V / m_e c^2$$

$$\Delta V = \eta(2\pi / cP)B_s h^2$$

$$n = n_{GJ} - n_{th} = \eta n_{GJ}$$

Charge number density

Goldreich-Julian (co-rotational) charge number density

$$n_{GJ} = 1.4\times10^{11}(B_s / B_d)(\dot{P}/10^{-15})^{0.5}\ P^{-0.5}\ cm^{-3}$$

Actual surface temperature of heated polar cap (2-4) MK

$$T_s = (2\times10^6\ K)\,P^{-0.25}\,(\dot{P}/10^{-15})^{0.25}\,\eta^{0.5}(B_s / B_d)^{0.5}(h/10^3\,cm)^{0.5}$$

$\overrightarrow{\Delta E} \times \vec{B}$ spark plasma circulation drift rate

Linear velocity of the E x B drift (RS75)

$$\upsilon_d = \frac{c\Delta E}{B_s} = \frac{c\eta(2\pi / cP)B_s h}{B_s} = \eta \frac{2\pi}{P} h \ \ [\mathrm{cm/s}]$$

B_s *-actual surface magnetic field*

B_d *-dipolar magnetic field at PC*

ΔE *- component of electric field caused by charge depletion* $\Delta\rho = \rho_{GJ} - \rho_{th} = \eta\rho_{GJ}$

$$\omega = \nu_d / d = \eta(2\pi / P)(h / d)$$

Carusel angular speed

Time interval to complete one circulation around periphery of PC

$$P_4 = \frac{2\pi d}{\upsilon_d}$$

$$P4 = \frac{P}{2\eta}\frac{d}{h} \leq \frac{P}{2\eta}\frac{r_p}{h}$$

Gil, Melikidze & Geppert 2003

$$d \leq r_{pc} = 1.4 (B_s / B_d)^{-1/2} 10^4 P^{1/2} \quad [\mathrm{cm}]$$

Within the model of the inner acceleration region to surface of the PC is heated to high temperatures by the back-flow of particles produced in sparking discharges.

The heating rate is determined by the same value of the electric field that is involved in the E x B drifting phenomenon.

thus, the observed drifting rate

$$P_4 = 2\pi d / \upsilon_d = \frac{P}{2\eta}\frac{d}{h} \leq \frac{P}{2\eta}\frac{r_p}{h}$$

and the observed heating rate (thermal X-ray luminosity from hot PC)

$$L_x = \sigma T_s^4 A_{bol} = \sigma T_s^4 A_{pc} (B_d / B_s)$$

should be strongly correlated.

Thermal X-ray luminosity from spark-heated polar cap

$$L_x = 2.5\times10^{31}\times(\dot{P}_{-15}/P^3)(P_4/P)^{-2}$$ ***erg/s***

Efficiency of thermal radiation from hot PC

$$L_x/\dot{E} = (0.63/I_{45})(P_4/P)^{-2}$$

$$\dot{E} = I\Omega\dot{\Omega}$$

Spin-down power

$$I = I_{45}10^{45}\ g\,cm^2$$

$$I_{45} = 1\pm0.15$$

Thermal efficiency is not directly sensitive to the bolometric surface area, *unlike the surface temperature and magnetic field (discussed in the previous talk)*

X-ray Multi Mirror (XMM) – Newton satelite telescope

One revolution on an excentric orbit around the Earth takes 48 hours – observations are not performed close to the Earth due to strong noise contamination

XMM-Newton observations of drifting subpulse PSR 0943+10

(Zhang, Sanwal & Pavlov 2005)

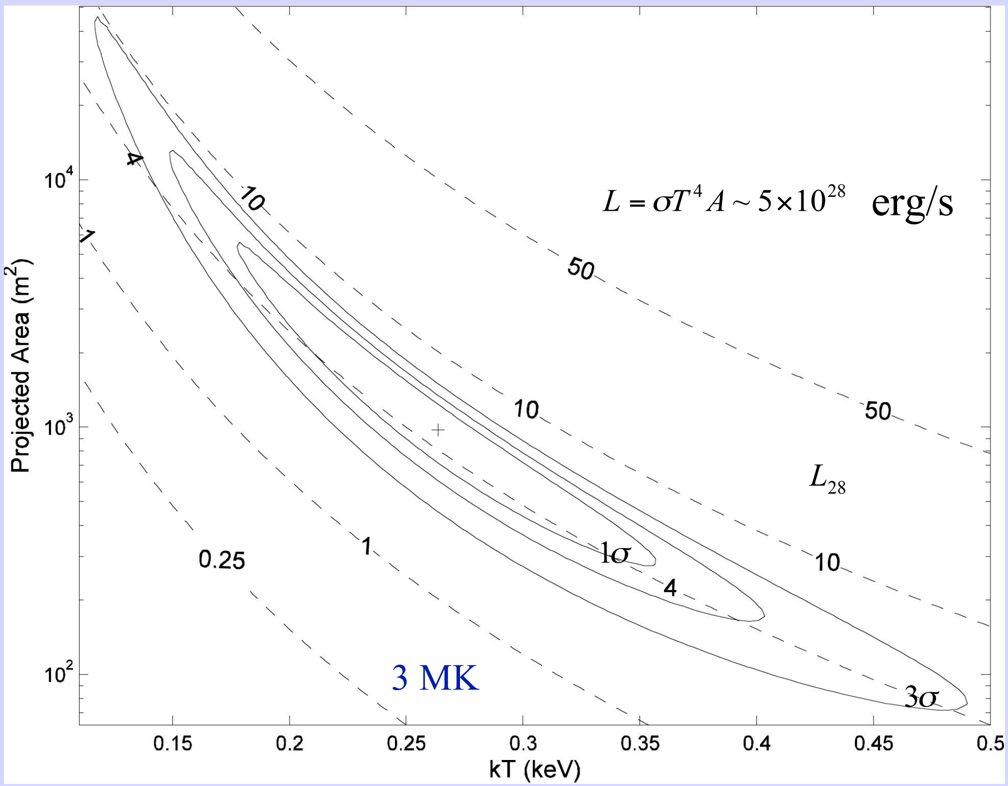

Consistent with thermal radiation from hot polar cap

Best BB fit:

A = 10^3(T/3MK)$^{-4}$ m^2
= (300 – 5000) m^2 ~1000 m^2

$A_{RS} = 6\times10^4\ \mathrm{m}^2$

T = (2.0-4.2) MK

$$L_x = \sigma T^4 A_{bol} \sim 5\times10^{28}\,\mathrm{erg/s}$$

68% confidence

$A \ll A_{RS}$

typical for thermal radiation from hot spots detected in a number of X-ray pulsars

$P_4 / P = 37.35$ **(radio)**

Poor photon statistics – magnetosperic X-ray emission could be fitted equally well

$$L_x / \dot{E} = 0.63\,(P_4 / P)^{-2}$$

D(kpc)

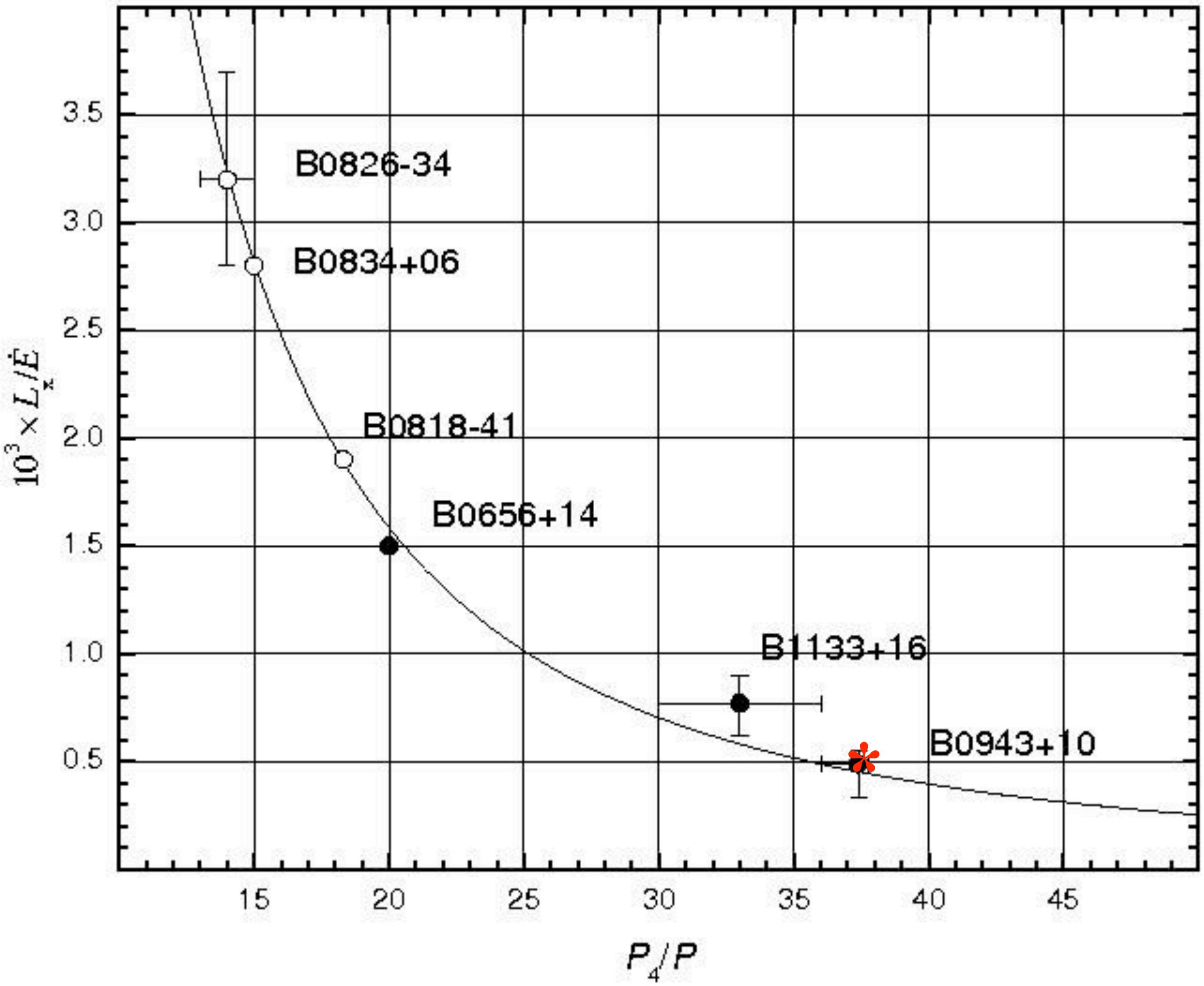

.432

.643

.257

.288

.350

.631

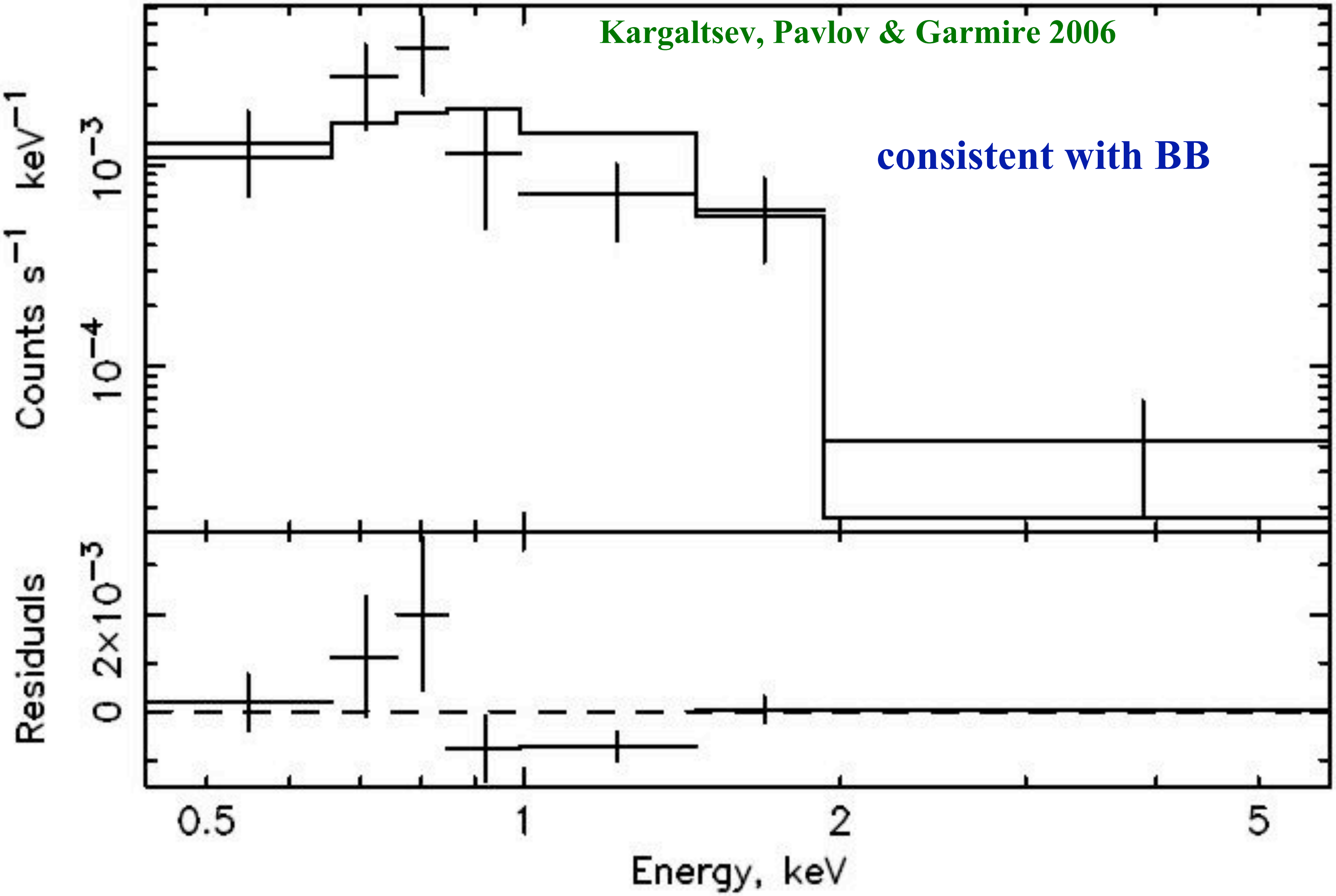

XMM-Newton spectrum of PSR B1133+16

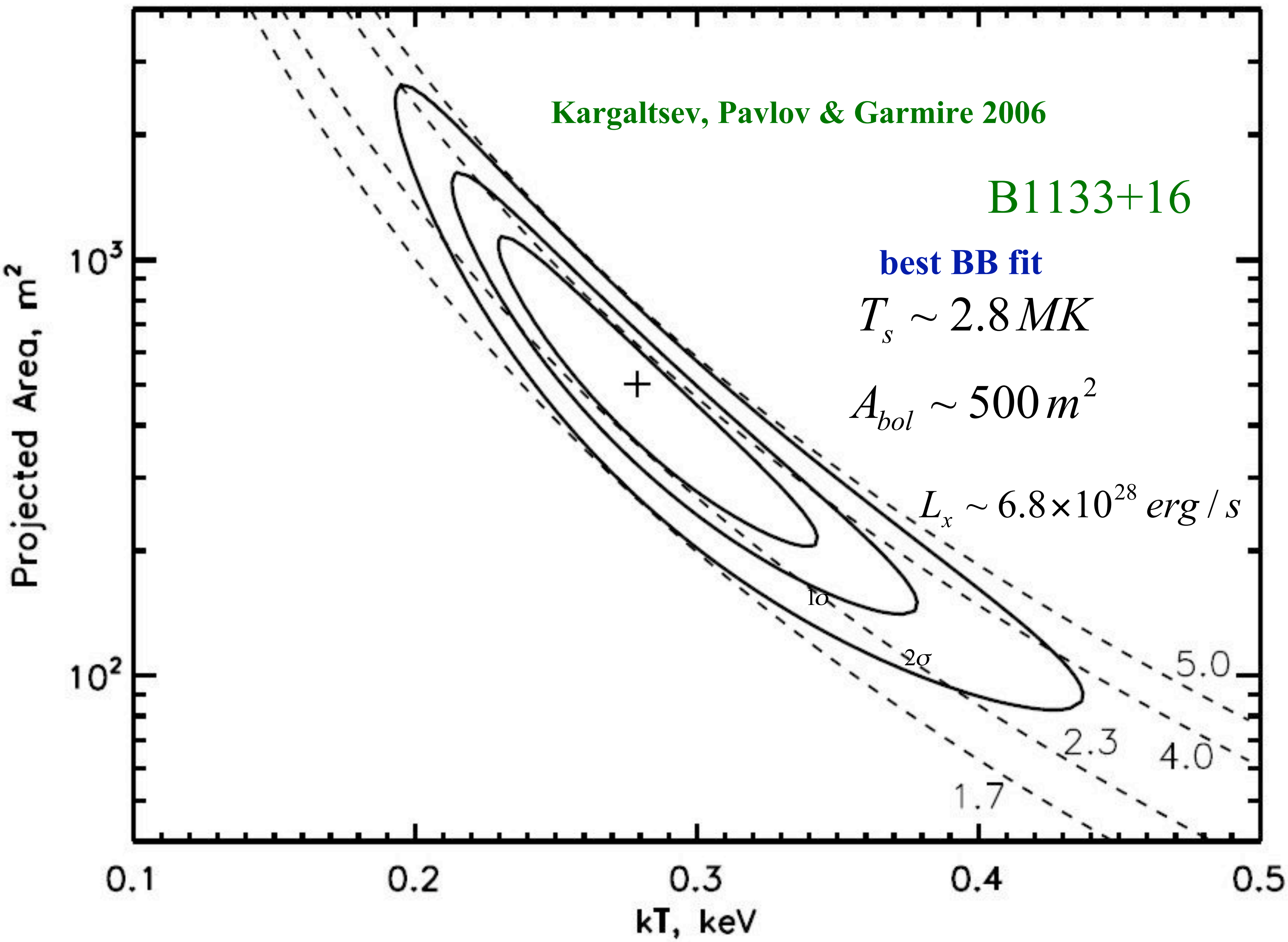

Better photon statistics; BB preferred over magnetospheric emission, but still no clear cut

Nowakowski, L., 1996, ApJ, 457,868

Weltevrede, Edwards And Stappers,. 2006

Fluctuation spectrum of PSR B1133+16

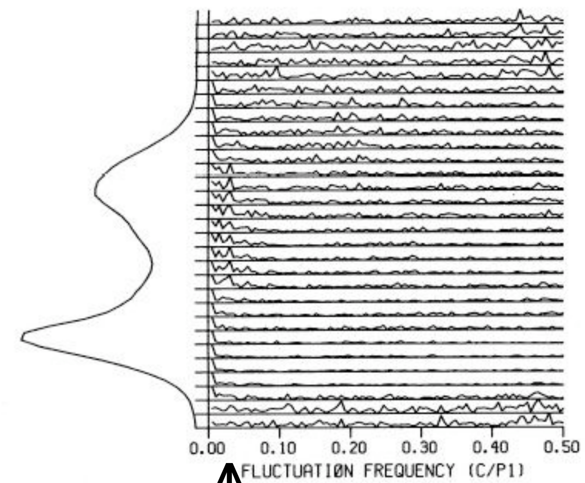

FIG. 10.—Longitude-resolved, unsmoothed power spectrum of PSR 1133+16 at 430 MHz. Thirty subwindows cover slightly more than the pulse window. Each power spectrum is individually normalized.

Single pulses

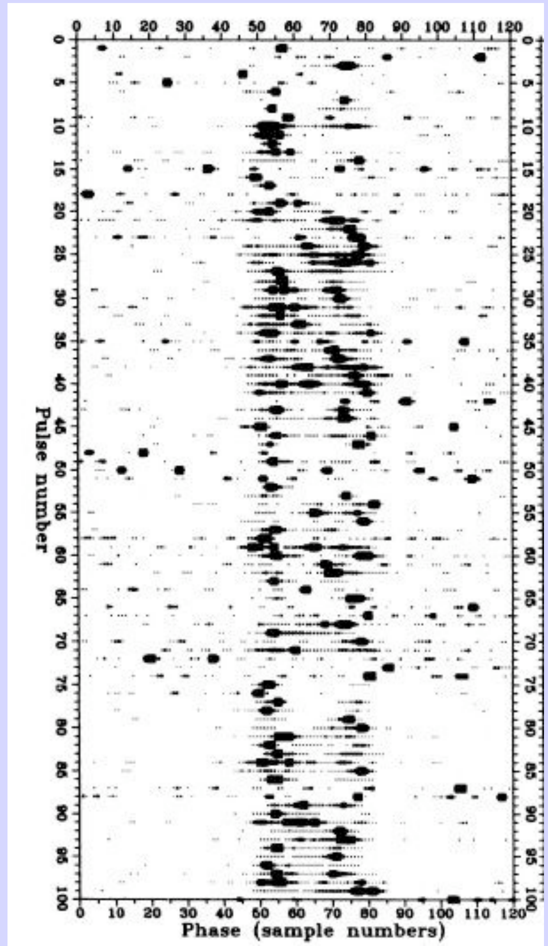

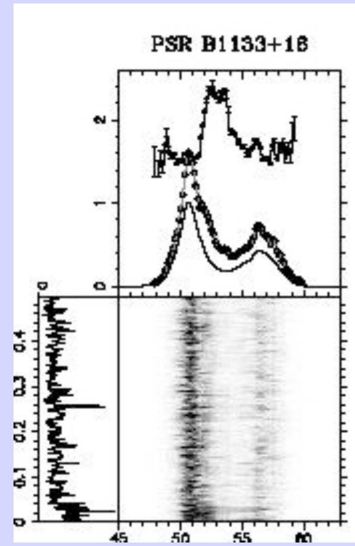

← *0.03 c/P*

$$P_4 / P = 33 \pm 3$$

Long period feature

0.031c/P => 32P

$$P_4 / P = 32 \quad ?$$

YES

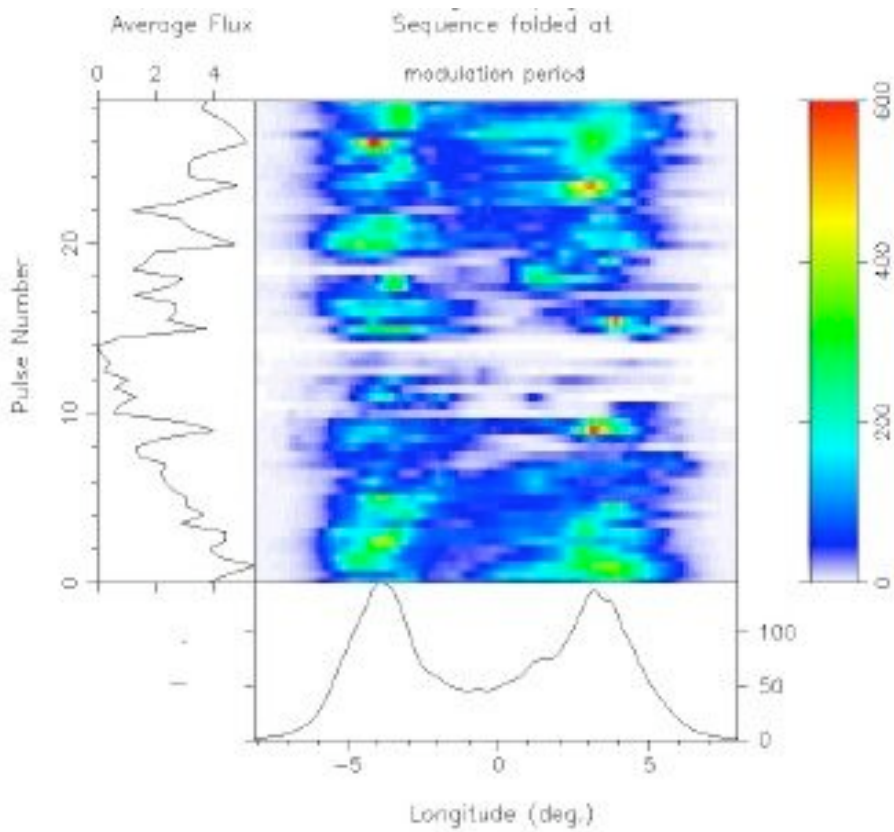

Figure 7. Typical 113-pulse intervals of observation (A in Table 1) folded at the local 28.44-P_1 putative value of $\hat{P}_3$. Each display represents the average of four such intervals. Note that both folded PSs show one or more "null zones" where the intensity is negligible as well as maxima that are 3-5 times larger than the average.

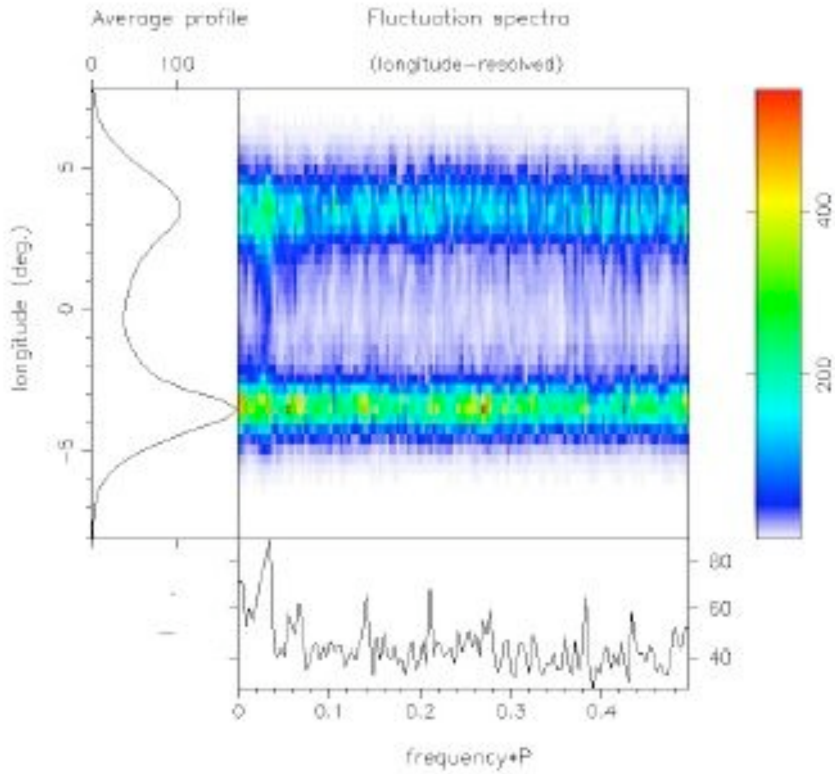

Figure 1. Typical longitude-resolved fluctuation spectra (hereafter LRF) for PSR B1133+16, computed in total power (Stokes I) for the 327-MHz observation ("D" in Table 1) on 2006 October 10. The main panel gives the spectra according to the average profile in the left panel, and the integrated spectrum is shown in the bottom panel. Here, an FFT length of 256 was used.

B1133+16

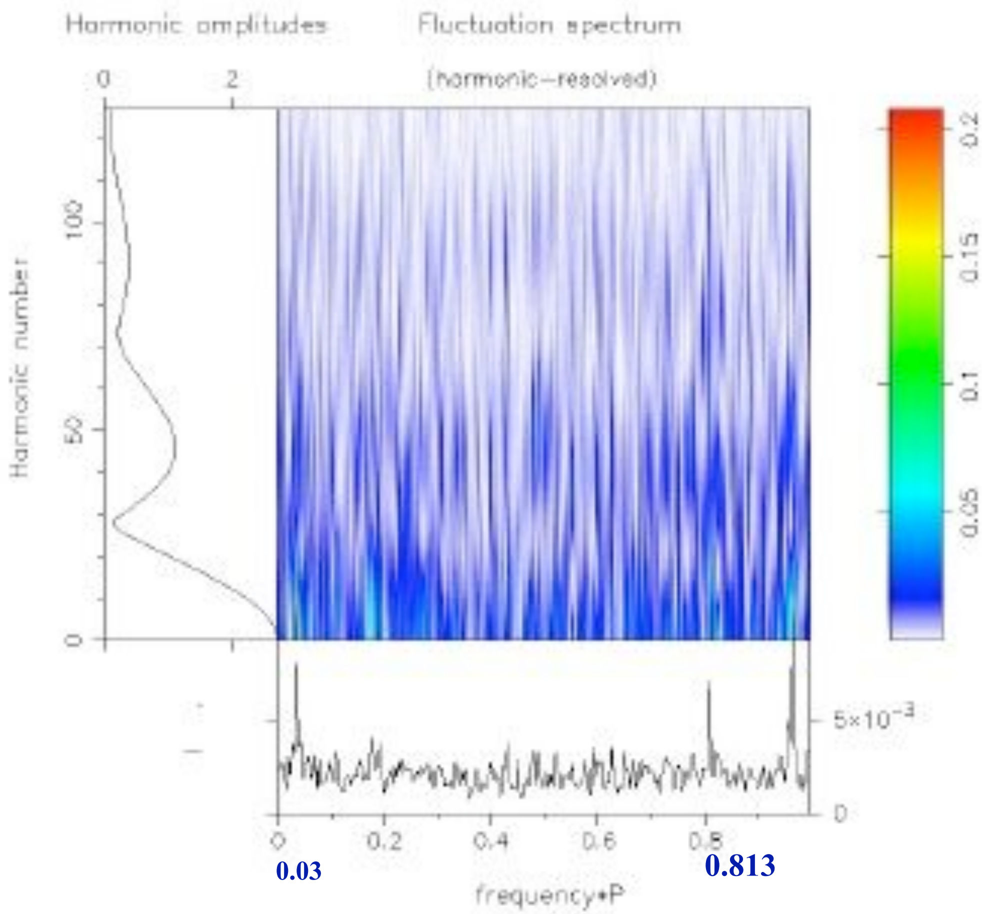

$$P_4 = 28.44P$$

$$N = P_4 / P_3 = 22.991 \pm 0.01 = 23$$

$$P_3 = (1.237 \pm 0.011)P$$

23 sub-beams

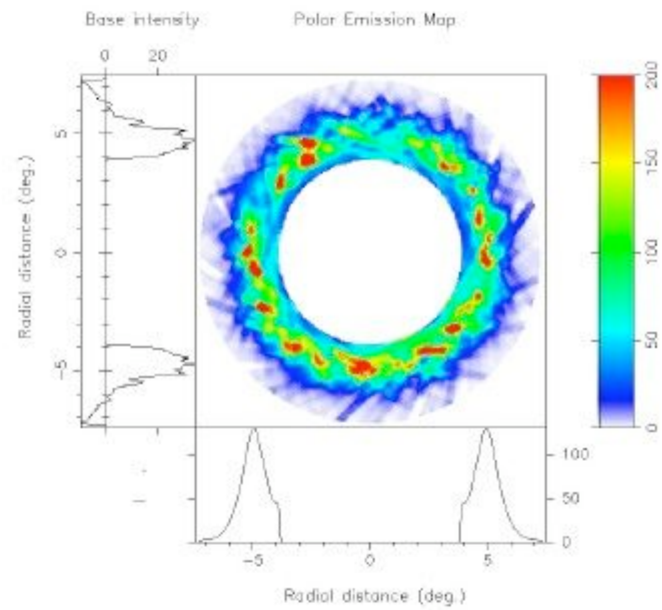

Figure A2. Polar map constructed using pulses 242-504 of the A PS. Here, $\hat{P}_3$ was determined to be 28.44 P_1, so the average of 7 carousel rotations is depicted. The magnetic axis is at the centre of the diagram, the "closer" rotational axis is upward, and (assuming a positive or equatorward traverse) the sightline track sweeps through the lower part of the pattern. Here, the star would rotate clockwise, causing the sightline to cut the counter-clockwise-rotating subbeam pattern from right to left; see DR01 for further details. The side panels give the "base" function (which has not been subtracted from the map), and the lower panel shows the radial form of the average beam pattern.

Rankin et al. 2007

$$L_x / \dot{E} = 0.63\,(P_4 / P)^{-2}$$

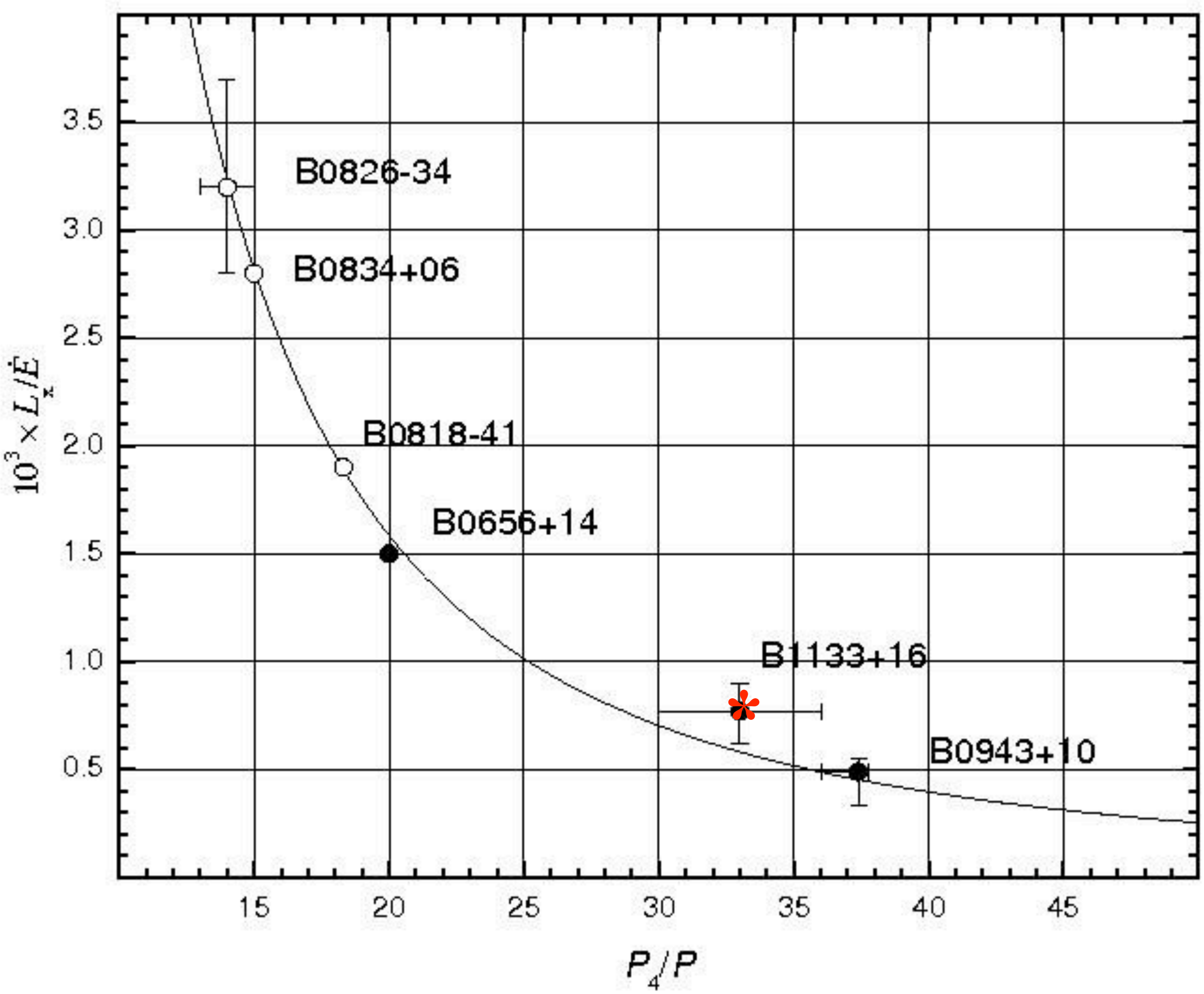

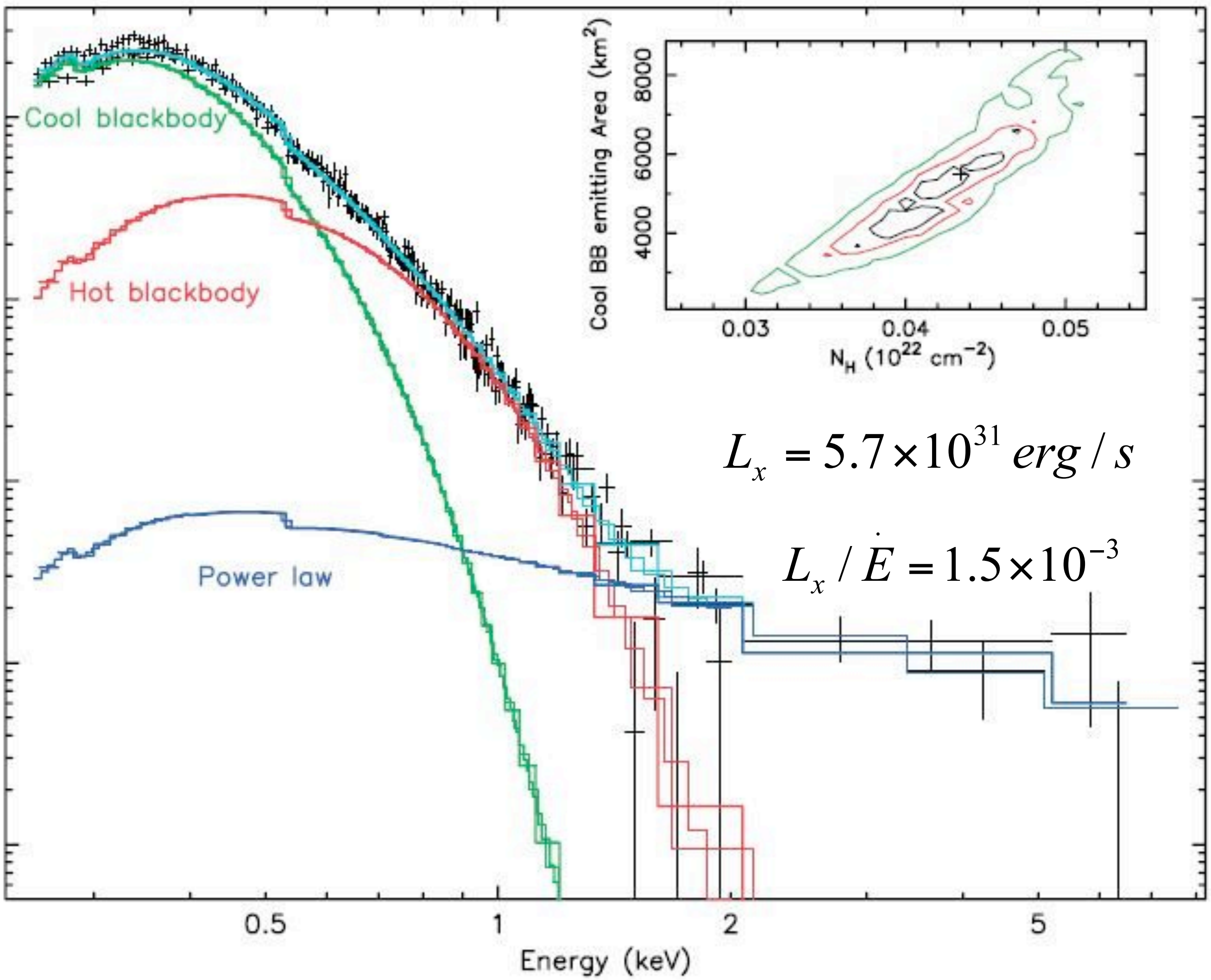

$$L_x = 5.7 \times 10^{31}\ erg / s$$

$$L_x / \dot{E} = 1.5 \times 10^{-3}$$

r PSR B0656+14. Data from pn (both small-window and fast-timing mode) and MOS1 are plotted (*black points*). Detailed values reported in Table 2.

Clear cut case

B0656+14

No question that hot blackbody originates on the Polar Cap

In radio band very erratic pulsar B0656+14

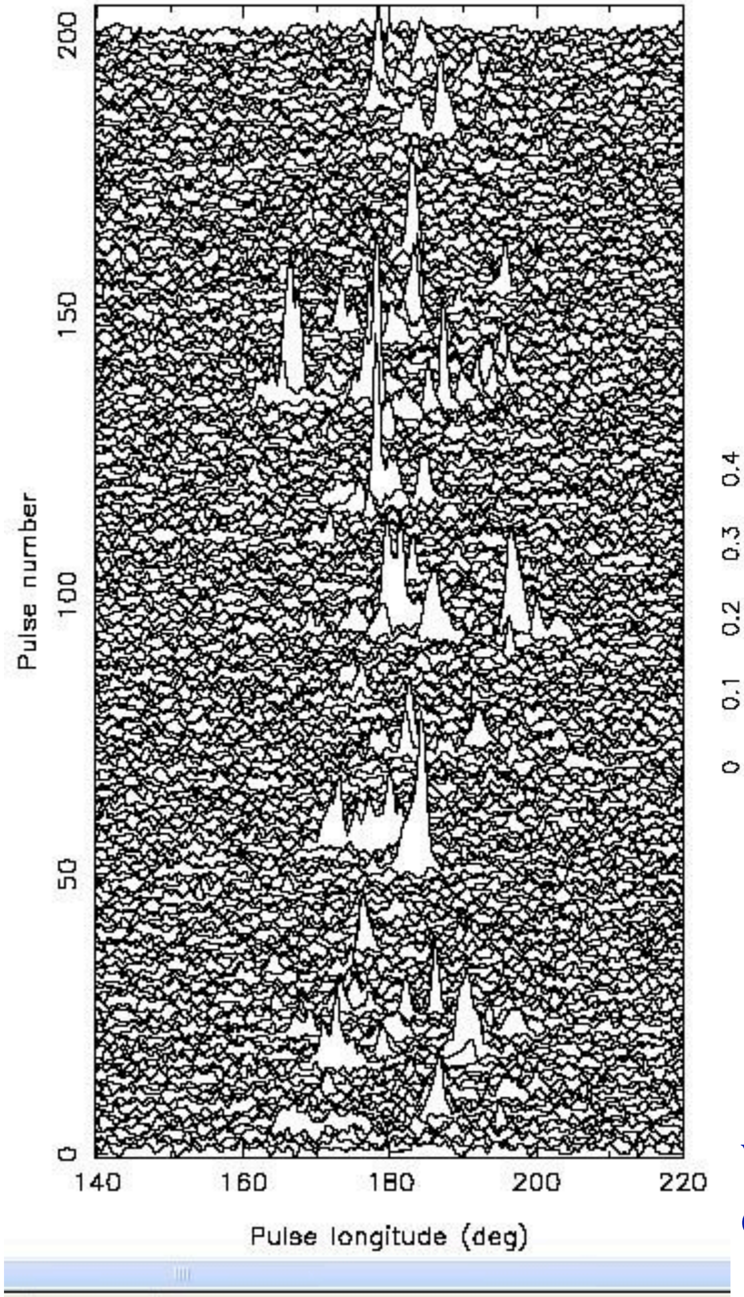

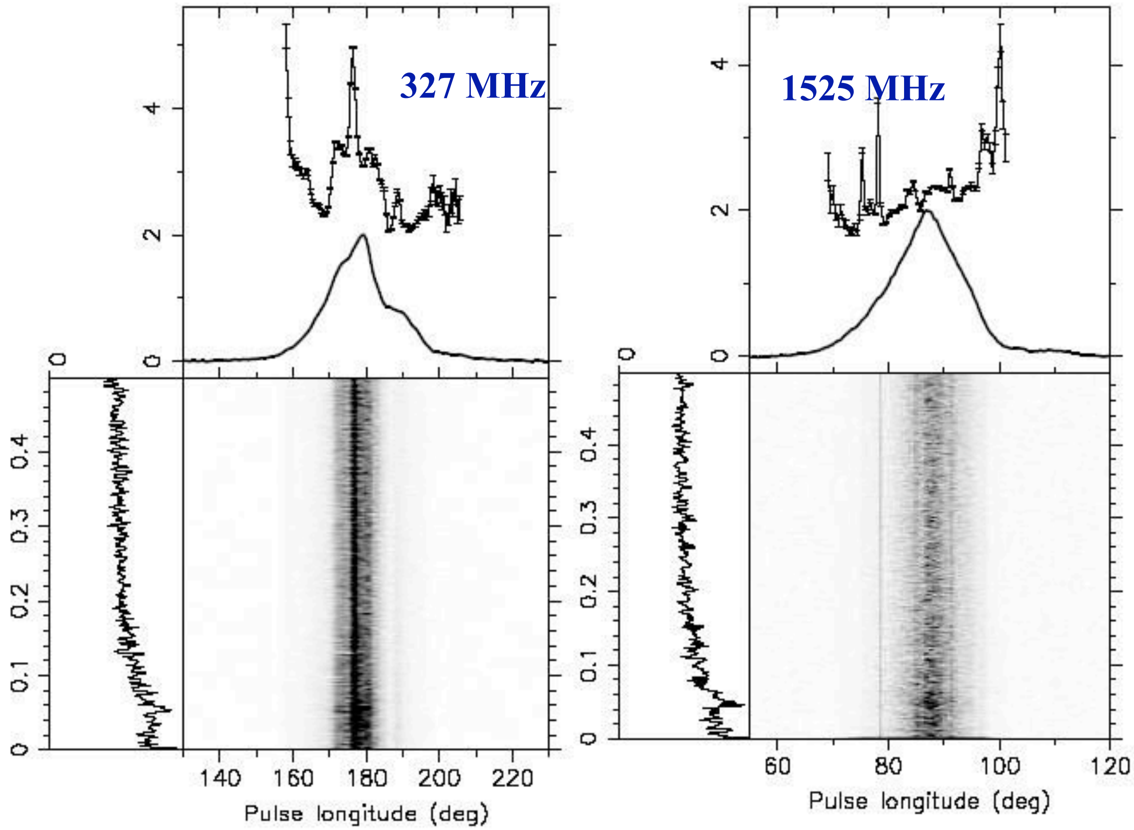

Clear intesity modulation feature at 20 P in the fluctuation spetrum

Weltevrede et al.. 2006

Q-mode or spiky mode

$$P_4 = 20P$$

$$L_x = 570\times10^{28} erg/s$$

$$L_x / \dot{E} = 0.63\,(P_4 / P)^{-2}$$

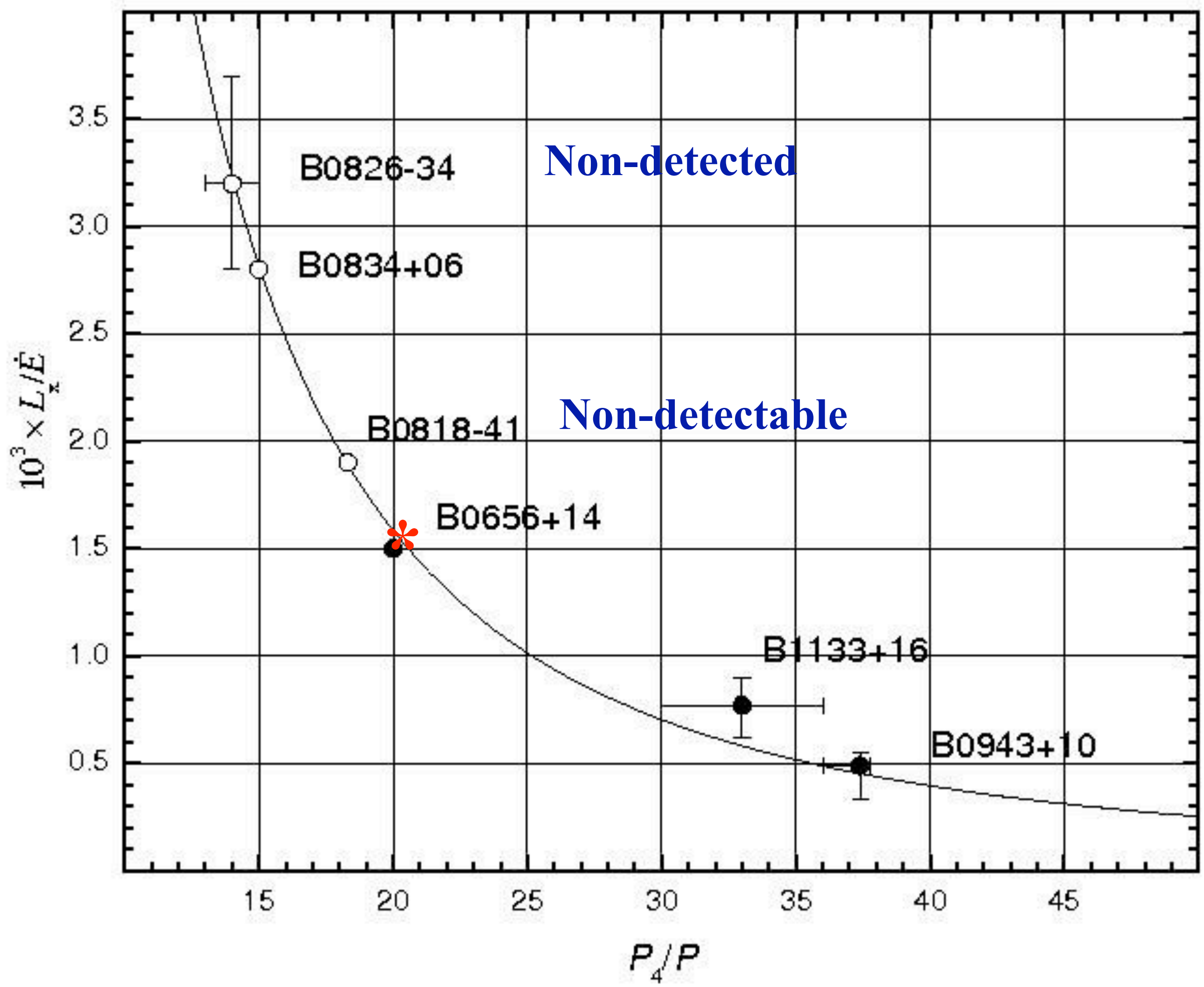

B0628-28   L_x=2.78 x 10^30 erg/s   E_dot=1.5 x 10^32 erg/s   ➔ P_4=(8+/-2) P

Weltevrede et al..2006

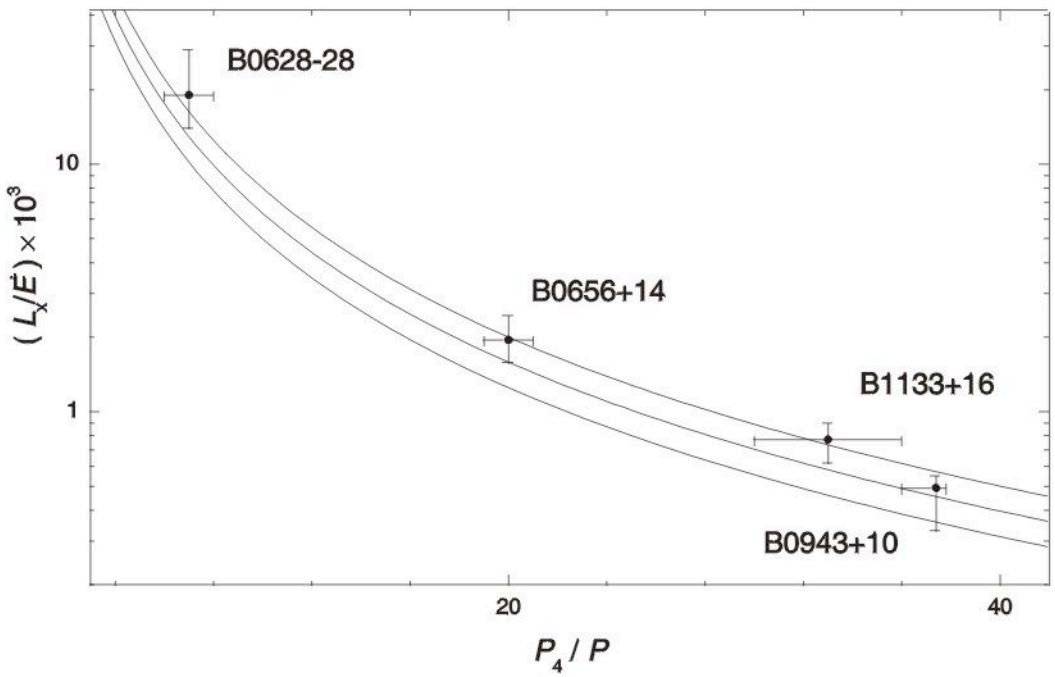

B0628-28
P_4=(8+/-2)P; Welevrede et al. 2006,
L_xbb; Ogelman 2005

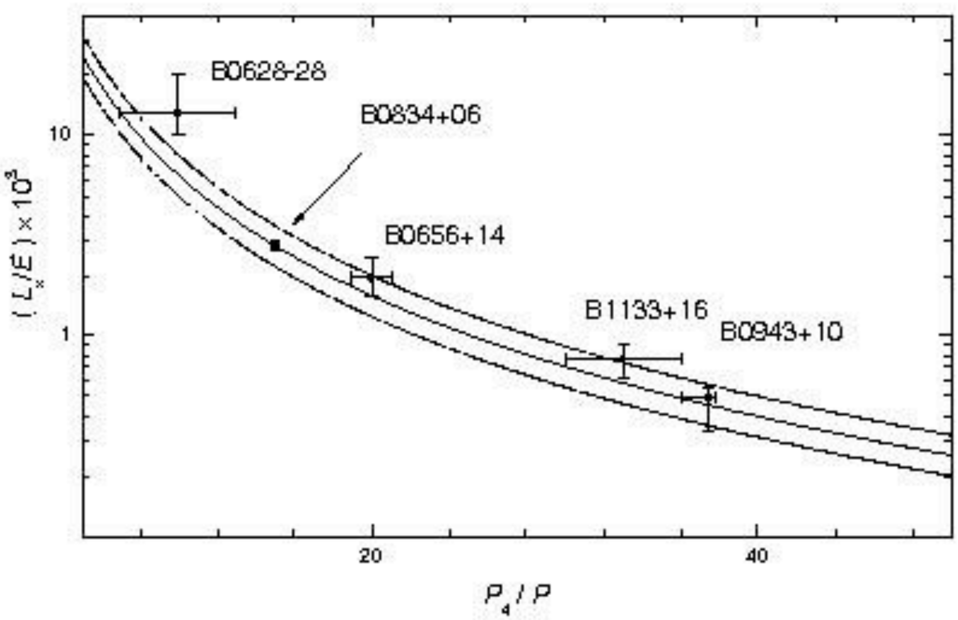

B0628-28
P_4=(10+/-3)P; Welevrede et al. 2007,
L_xbb; Becker 2005

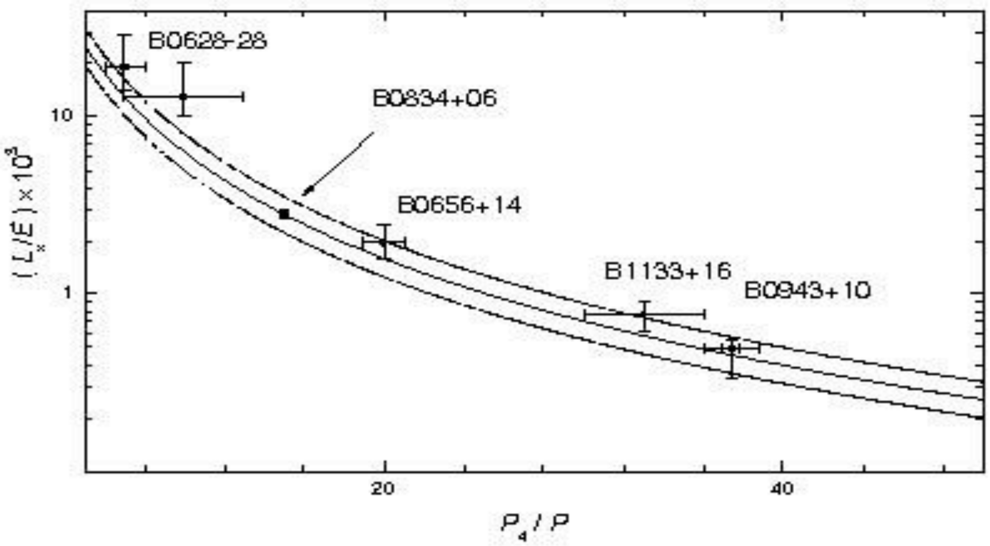

$$L_x / \dot{E} = 0.63 (P_4 / P)^{-2}$$

Gil, Melikidze & Zhang 2006

$$\eta = (1/2\pi)(P/P_3)$$

Screening factor ~(0.05-0.1)

only few % of GJ plasma involved in acceleration

$$L_x = 2.9\times10^{31}\times(\dot{P}_{-15}/P^3)(\hat{P}_3/P)^{-2} \quad \text{erg/s}$$

X-ray bolometric luminosity

$10^{(28-29)}$ erg/s

$$L_x/\dot{E} = 0.63(\hat{P}_3/P)^{-2}$$

Efficiency ~ 0.001

$$T_s = (8.2\times10^6\ K)\ A_4^{-0.25}\ \dot{P}_{-15}^{\ 0.25}\ P^{-0.75}\ (\hat{P}_3/P)^{-0.5}$$

$A_4 = A_{bol}/(10^4 m^2) \sim 0.1$

$T_s \sim (2-3)MK$

Name	$\hat{P}_3/P$		$L_x/\dot{E}\times10^{-3}$		$L_x\times10^{28}$		b	$T_s^{(obs)}$	$T_s^{(pred)}$	B_d	B_s
PSR B	Obs.	Pred.	Obs.	Pred.	Obs.	Pred.	A_{pc}/A_{bol}	10^6 K	10^6 K	10^{12}G	10^{14}G
0943 + 10	37.4	37	$0.5^{+0.2}_{-0.2}$	0.46	5^{+2}_{-2}	4.8	60^{+140}_{-48}	$3.1^{+0.9}_{-1.1}$	3^{+1}_{-1}	3.95	$2.37^{+5.53}_{-1.90}$
1133 + 16	(33^{+3}_{-3})	31^{+3}_{-2}	$0.77^{+0.13}_{-0.18}$	$1.0^{+0.3}_{-0.2}$	$7.7^{+1.3}_{-1.3}$	$8.9^{+1.3}_{-1.8}$	$11.1^{+16.6}_{-5.6}$	$2.8^{+1.2}_{-1.2}$	$2.4^{+0.8}_{-0.5}$	4.25	$0.47^{+0.71}_{-0.24}$
0826 − 34	14^{+1}_{-1}			$3.2^{+0.5}_{-0.4}$		$2.0^{+0.33}_{-0.25}$				2.74	
0834 + 06	15			2.8		37				5.94	

Future work

New XMM-Newton observations of PSR B0826-34
50 Ks performed in November 2006
Zhang, Gil, Melikidze, Geppert, Haberl

Non-detected $P_4 / P = 14 \pm 1$ **(Gupta, Gil, Kijak, Sendyk 2004)**

Proposal for XMM-Newton observations of
PSR B0834+06 accepted – observation in summer 2006
(simultaneous radio observations with GMRT planned)

Very promissing $P_4 / P = 15 \pm 1$ **(Asgekar, Deshapande 2005)**

Proposal for XMM-Newton observations of PSR B1702-19
will be submitted for the next cycle

Very promissing $P_4 / P = 10 \pm 1$ **(Weltevrede 2006; GMRT planned)**

B1702-19 5.0 .887 0.071

$$L_x / \dot{E} = 0.63\,(P_4 / P)^{-2}$$

D(kpc) n_H (10^22 /cm^2)

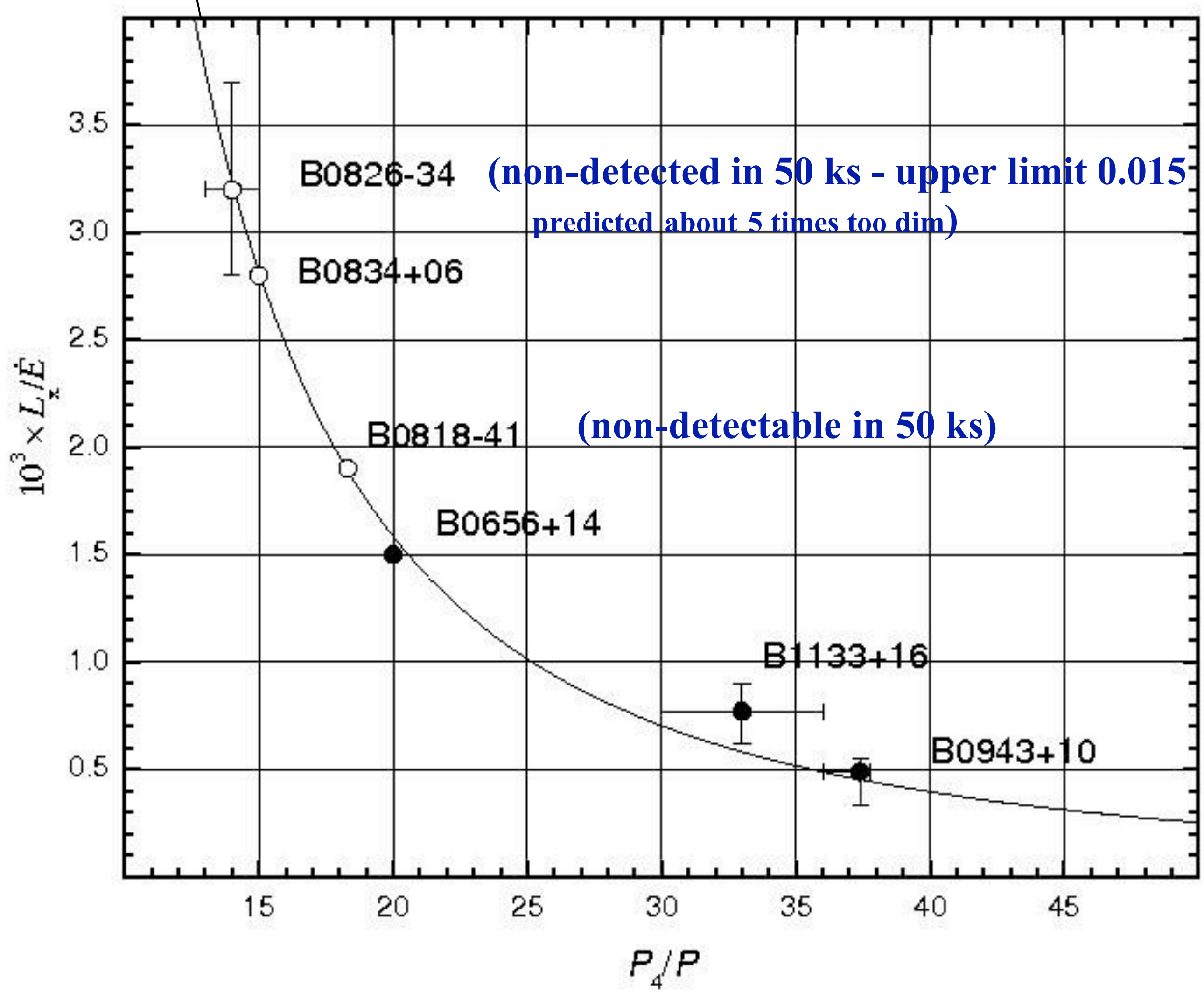

	D(kpc)	n_H (10^22 /cm^2)
B1702-19	.887	0.071
B0826-34	.432	1.45
B0834+06	.643	0.36
B0818-41	.257	3.42
B0656+14	.288	0.04
B1133+16	.350	0.015
B0943+10	.631	0.47

Non-detection of PSR B0826-34 in 50 ks XMM-Newton exposure

$$L_x / \dot{E} = 0.63 (P_4 / P)^{-2}$$

B0943+10

$$P_4 / P = 37$$

$$\dot{E} = 10^{32} \, erg/s$$

$$L_x = 5 \cdot 10^{28} \, erg/s$$

$$d = 630 \, pc$$

$$DM = 15; \quad n_H = 0.47 \cdot 10^{21}$$

B0826-34

$$P_4 / P = 14$$

$$\dot{E} = 6 \cdot 10^{30} \, erg/s$$

$$L_x = 3 \cdot 10^{28} \, erg/s$$ **?**

$$d = 430 \, pc$$

$$DM = 53; \quad n_H = 1.4 \cdot 10^{21}$$

Upper limit for B0826-34, assuming T~3 MK ➔ L_x > 1.4 10^29 erg/s
So this source with predicted bolometric L_x~3 10^28 erg/s could not be detected

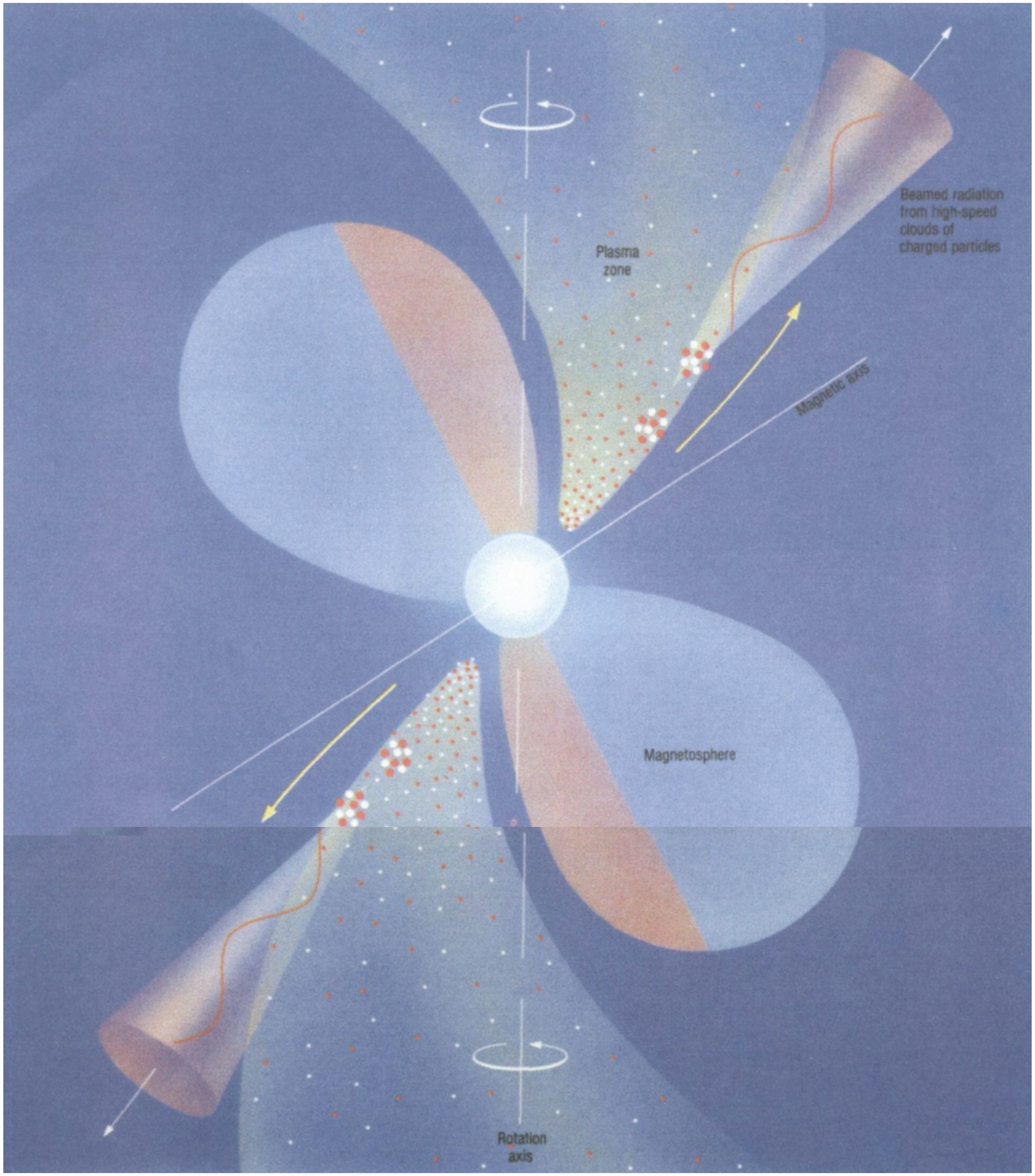
Beamed radiation
from high-speed
clouds of
charged particles
Plasma
zone
Magnetic axis
Magnetosphere
Rotation
axis

Polar gap model of B0943+10 consistent with XMM-Newton

(Gil, Melikidze & Geppert 2003, Zhang, Sanwal & Pavlov 2005; Gil, Melikidze & Zhang 2006)

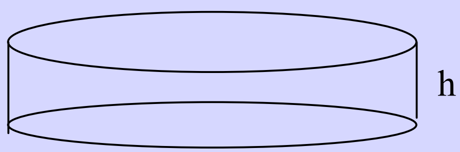

Pure VG – too luminous in X-ray
SCLF – too dim in X-ray

Partially screened gap gives

- right bolometric area $A = 10^7\ cm^2$
- right surface temperature T~3 MK
- right drift periodicity $\hat{P}_3/P \sim 37$

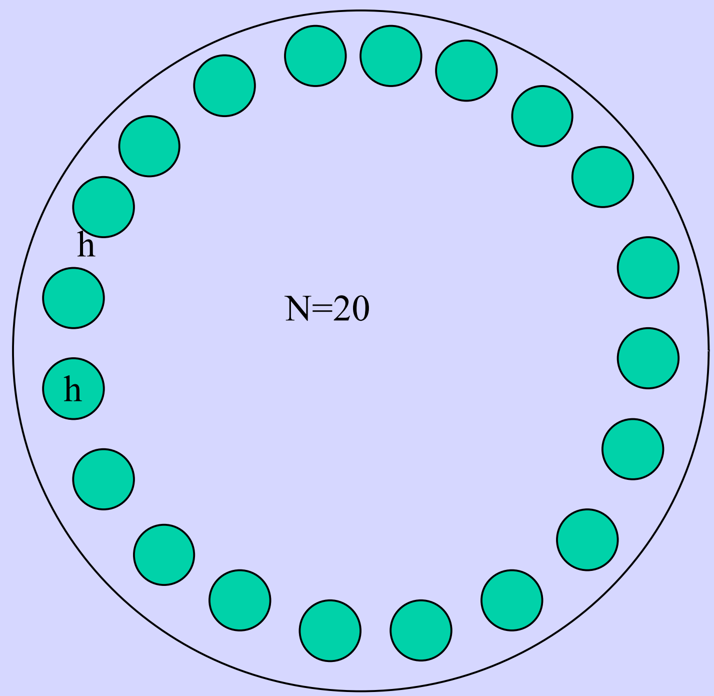

Characteristic spark dimension ~ h

Co-rotating magnetosphere

$$E_c = -(\Omega \times r / c) \times B_s$$

Force-free magnetosphere

$$E_c \cdot B_s = 0$$

$\Delta V_{\|} = 0$

No acceleration along *B*

GJ69, RS75

$$\rho_c = (1/2\pi)\, divE_c =$$

$$= -\Omega \cdot B_s /(2\pi c) = \pm B_s / cP$$

Co-rotating charge density

$$\upsilon_{cor} = c(E_c \times B_s) / B^2 = cE_c / B_s$$

Linear co-rotation velocity

Name	$\hat{P}_3/P$		$L_x/\dot{E} \times 10^{-3}$		$L_x \times 10^{28}$		b	$T_s^{(obs)}$	$T_s^{(pred)}$	B_d	B_s
PSR B	Obs.	Pred.	Obs.	Pred.	Obs.	Pred.	A_{pc}/A_{bol}	10^6 K	10^6 K	10^{12}G	10^{14}G
0943 + 10	37.4	37	$0.5^{+0.2}_{-0.2}$	0.46	5^{+2}_{-2}	4.8	60^{+140}_{-48}	$3.1^{+0.9}_{-1.1}$	3^{+1}_{-1}	3.95	$2.37^{+5.53}_{-1.90}$
1133 + 16	(33^{+3})	31^{+3}	$0.77^{+0.13}$	$1.0^{+0.3}$	$7.7^{+1.3}$	$8.9^{+1.3}$	$11.1^{+16.6}$	$2.8^{+1.2}$	$2.4^{+0.8}$	4.25	$0.47^{+0.71}$

The only two cases existing with both measurements

B1133+16 $L_x/\dot{E} \sim 0.77 \times 10^{-3}$ $\hat{P}_3/P \sim 33$

B0943+10 $L_x/\dot{E} \sim 0.5 \times 10^{-3}$ $\hat{P}_3/P \sim 37$

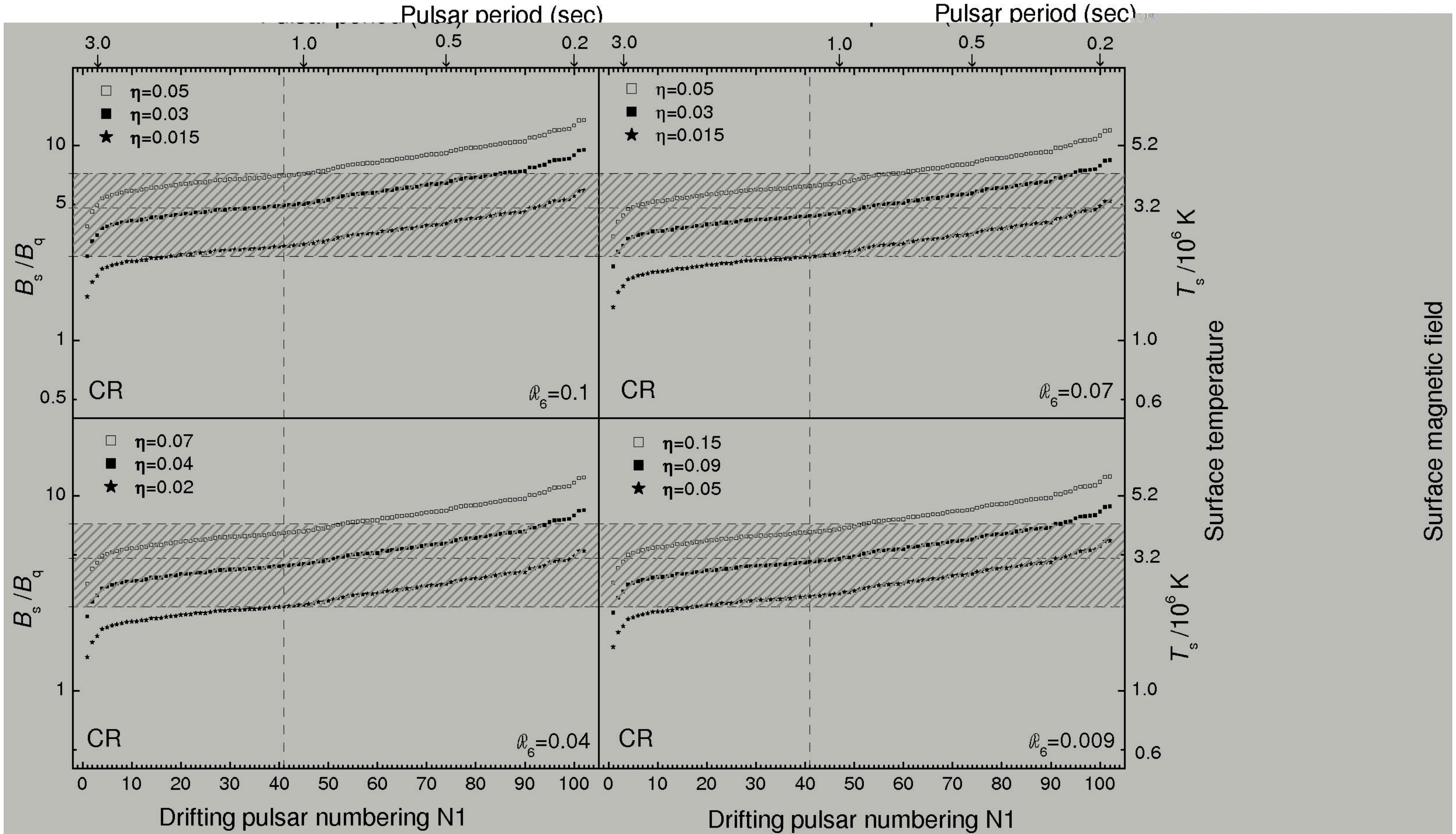

Pulsar period (sec)
3.0
1.0
0.5
0.2
η=0.05
η=0.03
η=0.015
η=0.07
η=0.04
η=0.02
η=0.15
η=0.09
η=0.05
CR
$\mathcal{R}_6$=0.1
$\mathcal{R}_6$=0.07
$\mathcal{R}_6$=0.04
$\mathcal{R}_6$=0.009
B_s/B_q
$T_s/10^6$ K
Surface temperature
Surface magnetic field
Drifting pulsar numbering N1

Gil, Melikidze & Zhang 2006

$$\eta = (1/2\pi)(P/P_3)$$

Screening factor ~(0.05-0.1)

only few % of GJ plasma involved in acceleration

$$L_x = 2.9\times 10^{31} \times (\dot{P}_{-15}/P^3)(\hat{P}_3/P)^{-2} \quad \text{erg/s}$$

X-ray bolometric luminosity

$10^{(28-29)}$ erg/s

$$L_x/\dot{E} = 0.63(\hat{P}_3/P)^{-2}$$

Efficiency ~ 0.001

$$T_s = (8.2\times 10^6\ K)\ A_4^{-0.25}\ \dot{P}_{-15}^{\ 0.25}\ P^{-0.75}\ (\hat{P}_3/P)^{-0.5}$$

$A_4 = A_{bol}/(10^4 m^2) \sim 0.1$

$T_s \sim (2-3)MK$

Name	$\hat{P}_3/P$		$L_x/\dot{E}\times 10^{-3}$		$L_x \times 10^{28}$		b	$T_s^{(obs)}$	$T_s^{(pred)}$	B_d	B_s
PSR B	Obs.	Pred.	Obs.	Pred.	Obs.	Pred.	A_{pc}/A_{bol}	10^6 K	10^6 K	10^{12}G	10^{14}G
0943 + 10	37.4	37	$0.5^{+0.2}_{-0.2}$	0.46	5^{+2}_{-2}	4.8	60^{+140}_{-48}	$3.1^{+0.9}_{-1.1}$	3^{+1}_{-1}	3.95	$2.37^{+5.53}_{-1.90}$
1133 + 16	(33^{+3}_{-3})	31^{+3}_{-2}	$0.77^{+0.13}_{-0.18}$	$1.0^{+0.3}_{-0.2}$	$7.7^{+1.3}_{-1.3}$	$8.9^{+1.3}_{-1.8}$	$11.1^{+16.6}_{-5.6}$	$2.8^{+1.2}_{-1.2}$	$2.4^{+0.8}_{-0.5}$	4.25	$0.47^{+0.71}_{-0.24}$
0826 − 34	14^{+1}_{-1}			$3.2^{+0.5}_{-0.4}$		$2.0^{+0.33}_{-0.25}$				2.74	
0834 + 06	15			2.8		37				5.94	

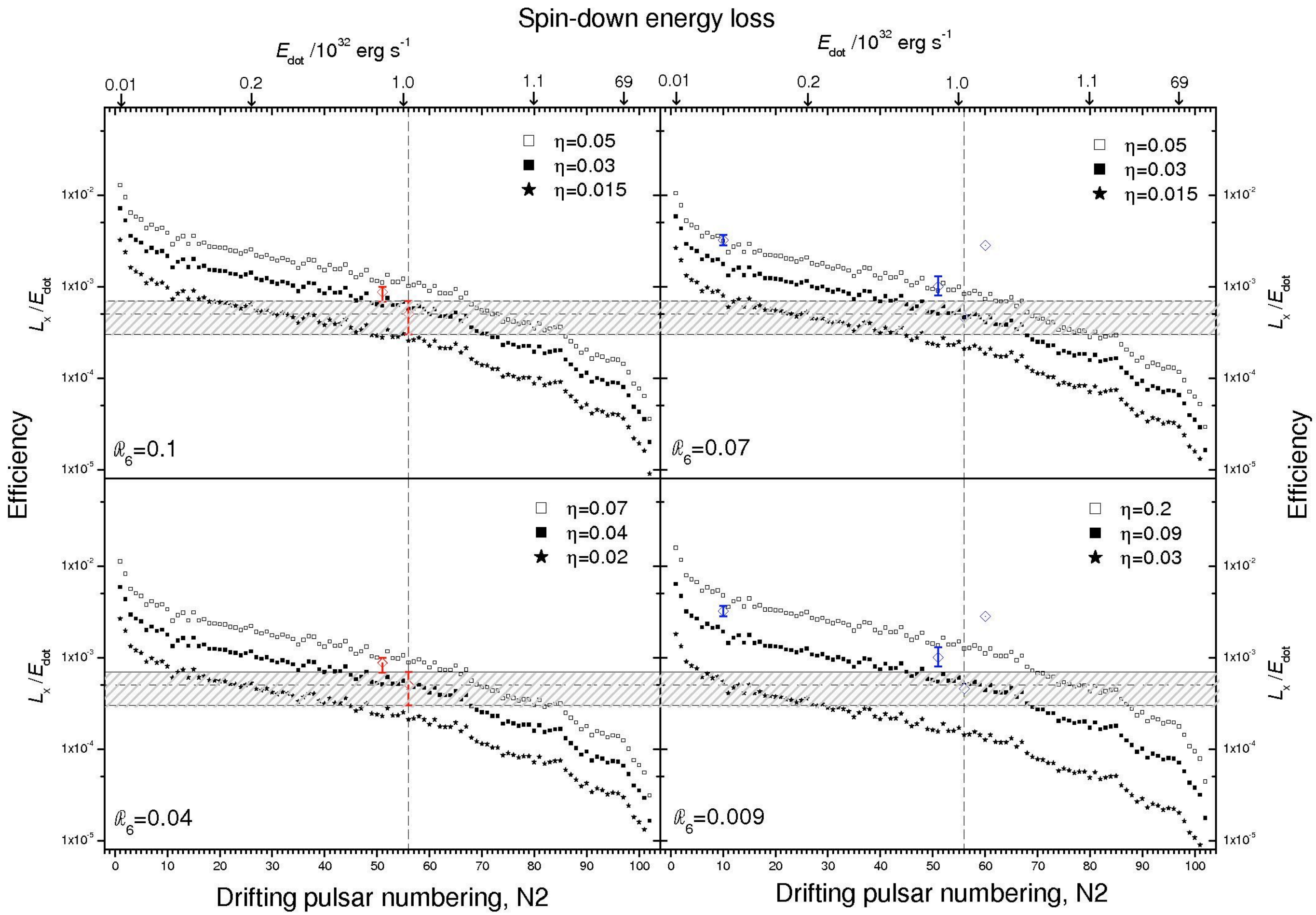

Spin-down energy loss
E_{dot} /10^{32} erg s^{-1}
0.01
0.2
1.0
1.1
69
η=0.05
η=0.03
η=0.015
$\mathcal{R}_6$=0.1
$\mathcal{R}_6$=0.07
η=0.07
η=0.04
η=0.02
$\mathcal{R}_6$=0.04
η=0.2
η=0.09
η=0.03
$\mathcal{R}_6$=0.009
L_x / E_{dot}
Efficiency
Drifting pulsar numbering, N2

Internal structure of the pulsar beam reflected in complex shapes of single pulses and/or mean profiles
(some degree of symmetry in profiles)
(correlations with the impact angle)

Nested cones | Patches

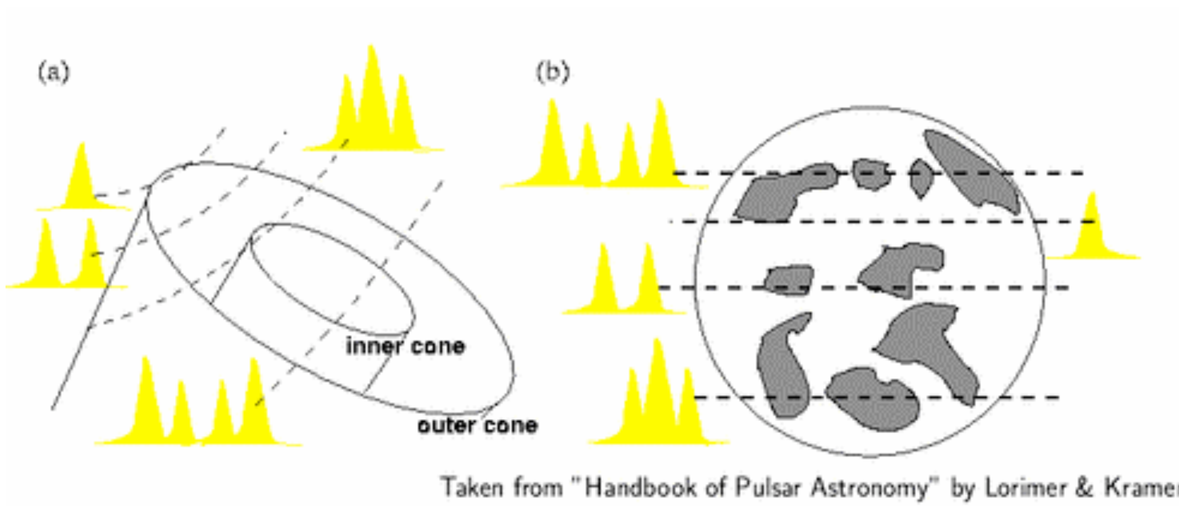

Rankin 1993, Gil et al. 1993 | Lyne & Manchester 1988

Rotating, magnetized Neutron Star

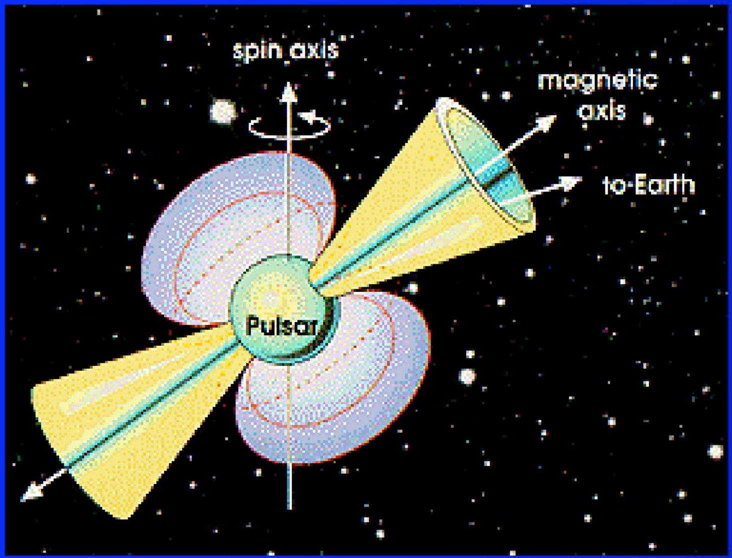

Pulsar

Internal beam structure

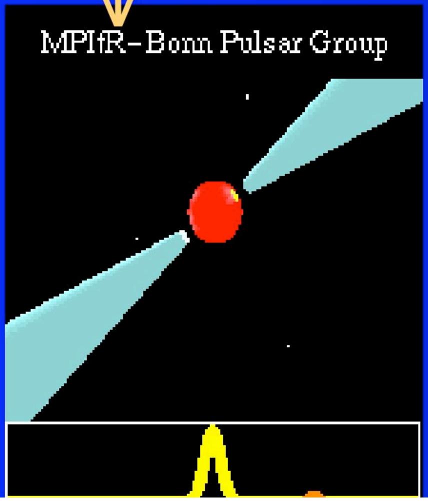

Complex pulse shapes

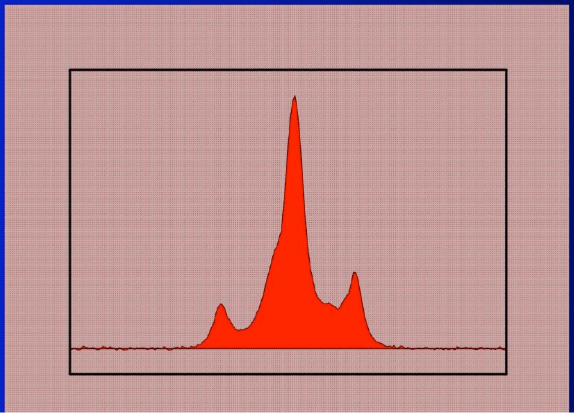

40 years after discovery of pulsars the actual mechanism of their coherent radio emission is still a mystery.

Drifting subpulses, which seem to be a common phenomenon in pulsar radiation, is also a puzzle.

„The mechanism for drifting subpulses cannot be very different from the mechanism of observed radio emission ...

...intrinsic property of radiation mechanism „

(Weltevrede, Edwards & Stappers 2006, A&A 445,243)

B0943+10

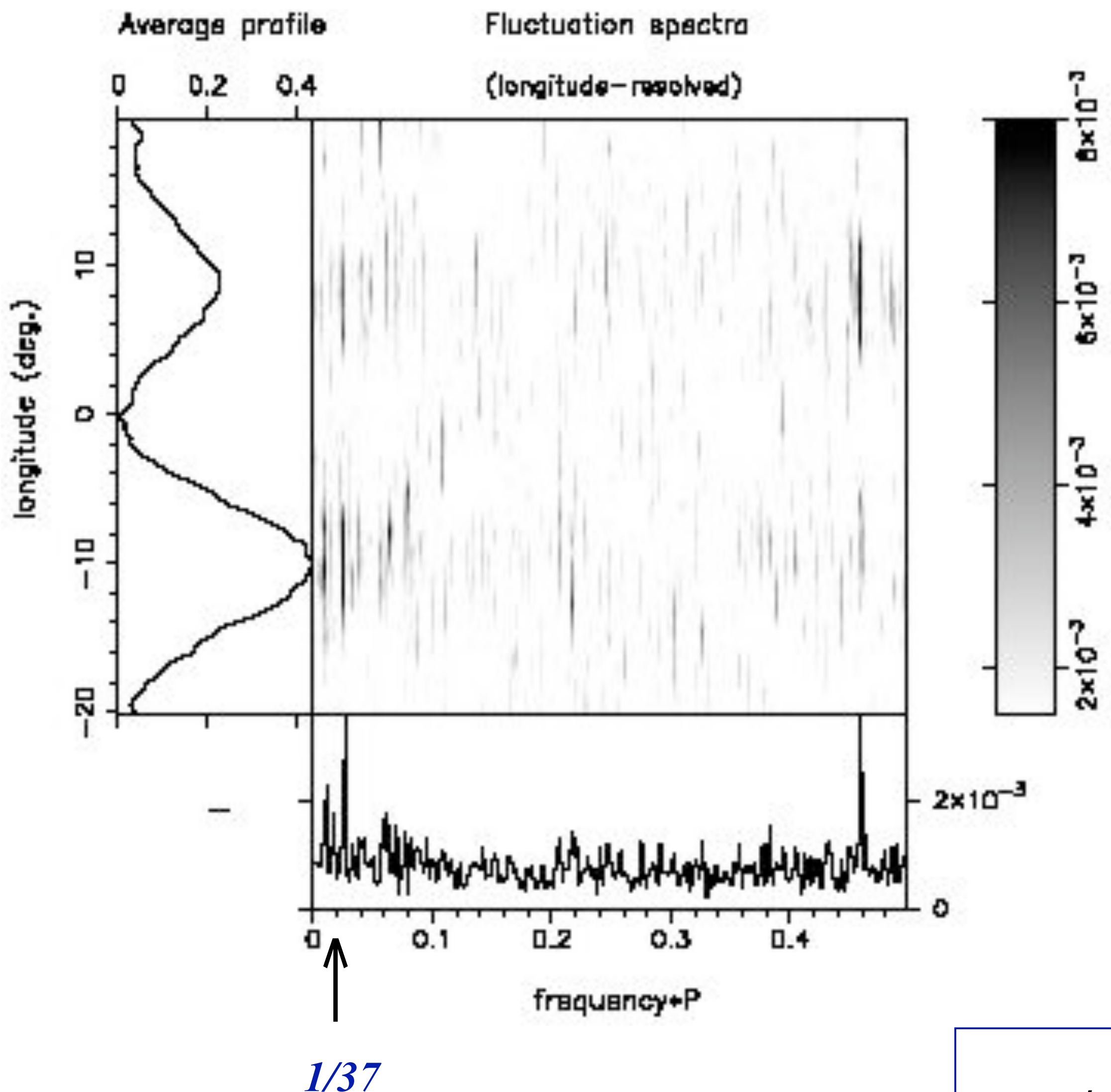

Deshpande
Rankin
Asgekar
1999,2001,2005

$$P_4 / P \sim 37$$

Possible interrelation between radio and X-ray signatures of drifting subpulses in pulsars

L_x **versus** P_4

Thermal (bolometric) luminosity from polar cap heated by sparks associated with (drifting) subpulses

$$L_x = \sigma T_s^4 A_{bol} = \sigma T_s^4 A_{pc} (B_d / B_s)$$

Tertiary (carousel) subpulse drift periodicity → circulation period of subpulse associated sparks

$$P_4 \approx 2\pi r_p / \upsilon_d$$

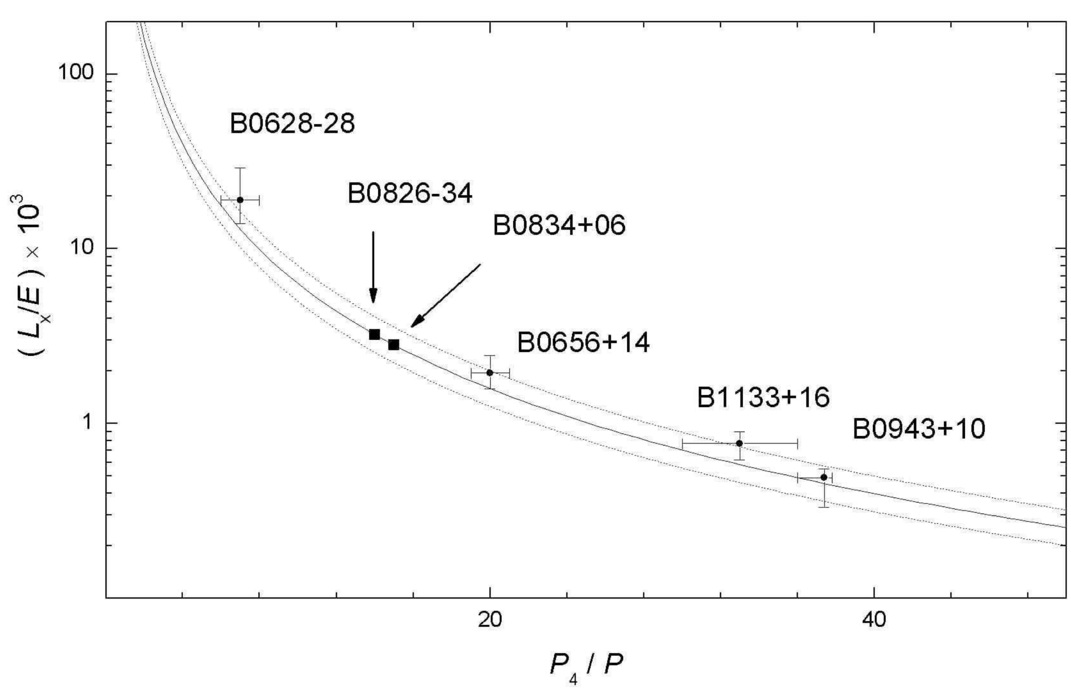

B0628-28
B0826-34
B0834+06
B0656+14
B1133+16
B0943+10
100
10
1
20
40
(L_x/E) × 10^3
P_4 / P

Sparking discharge of charge depleted acceleration region

Potential drop $10^{11-12}\,V$ exceeds threshold for the magnetic pair production – cascade developes until corotational charge is rebuild – this restores corotation for short time *t~h/c~(10-100)ns*

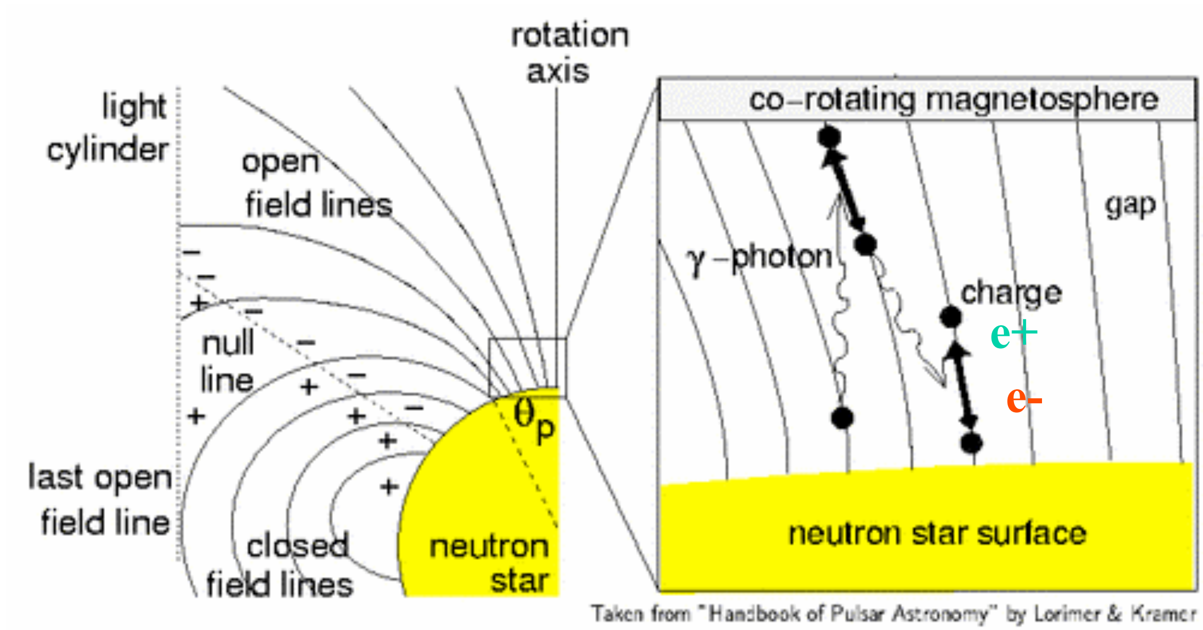

$\Delta V(h)$

h

Gap height *h* determined by the mean free path of photons for the magnetic pair production. The accelerating potential drop

$$\Delta Ve = \frac{2\pi e}{cP} B_s h^2 \sim 10^6\, MeV$$

is the energy reservuar to power the pulsar radiation

Inner acceleration region and structure of surface magnetic field B_s

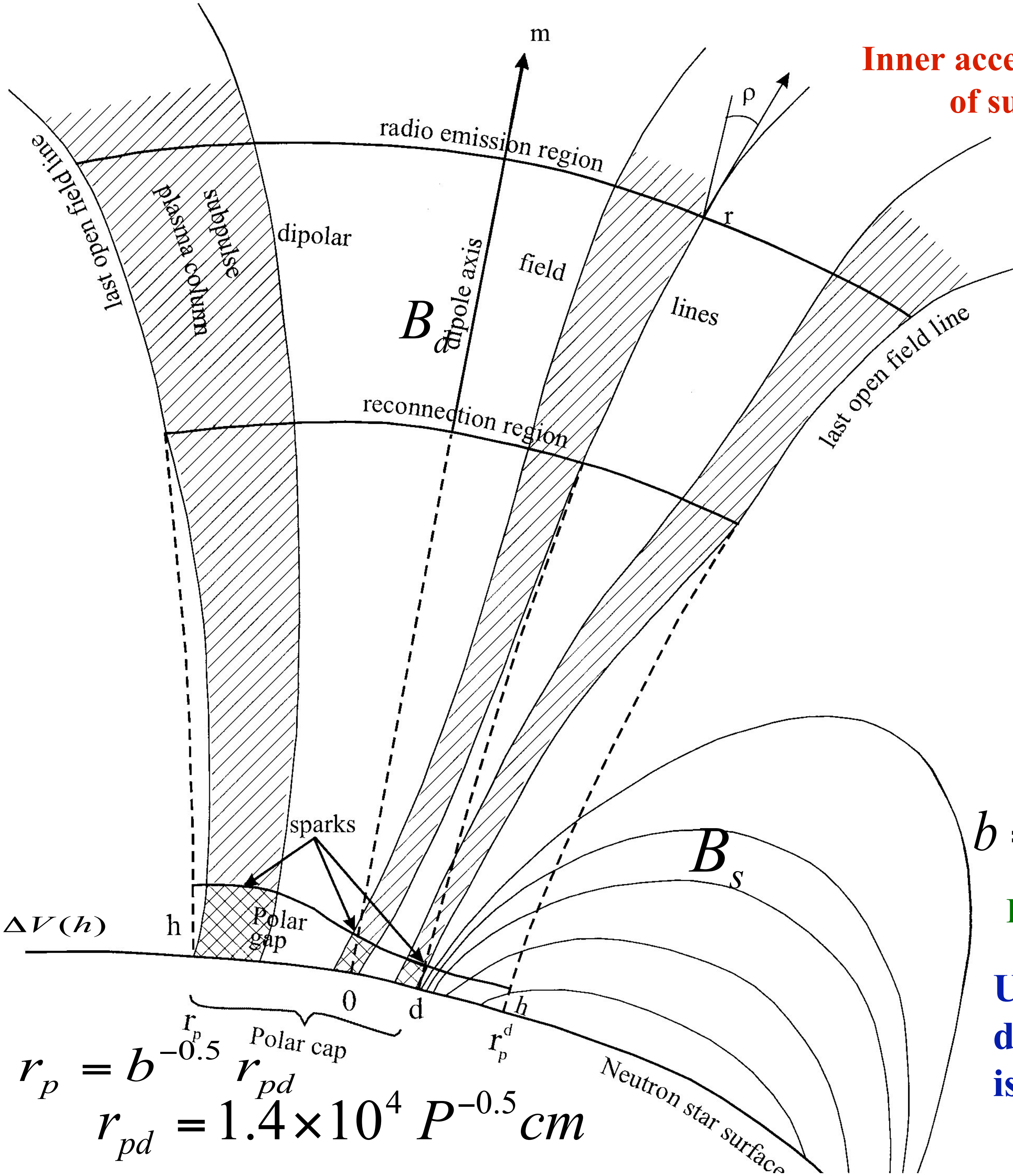

$$r_p = b^{-0.5}\ r_{pd}$$

$$r_{pd} = 1.4 \times 10^4\ P^{-0.5}\ cm$$

Assume:

Strong non-dipolar surface magnetic field

Consistent with:

Spectral lines

Small bolometric PC areas compared with canonical values

$$b = B_s / B_d = A_{pc} / A_{bol}$$

Ruderman & Sutherland 1975

Ultra-high gap potential drop discharges via a number of isolated spark filaments

101 pulsars with detected drifting subpulses

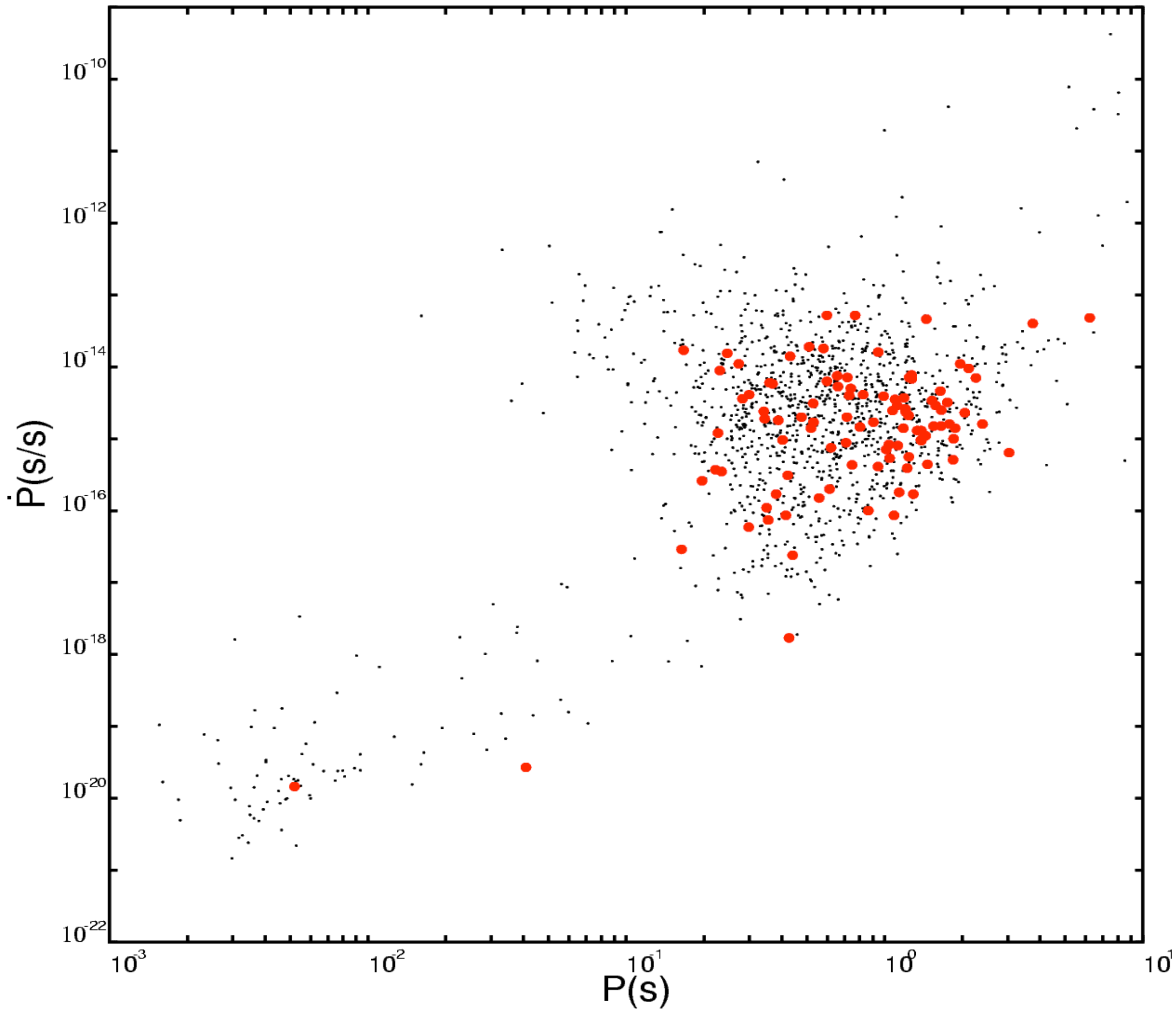

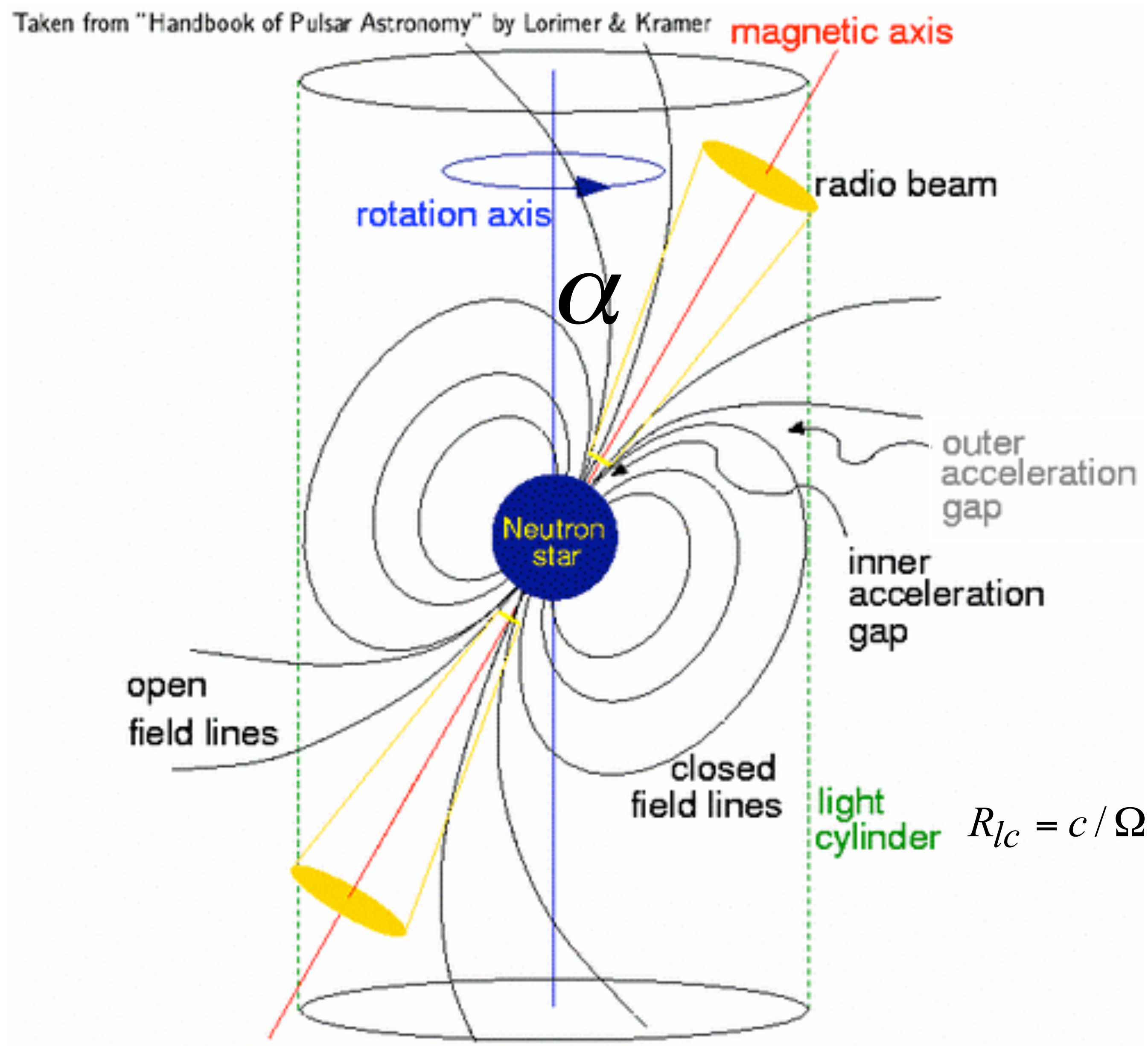

$$R_{lc} = c / \Omega = cP / 2\pi$$

Zoom on the Polar Cap

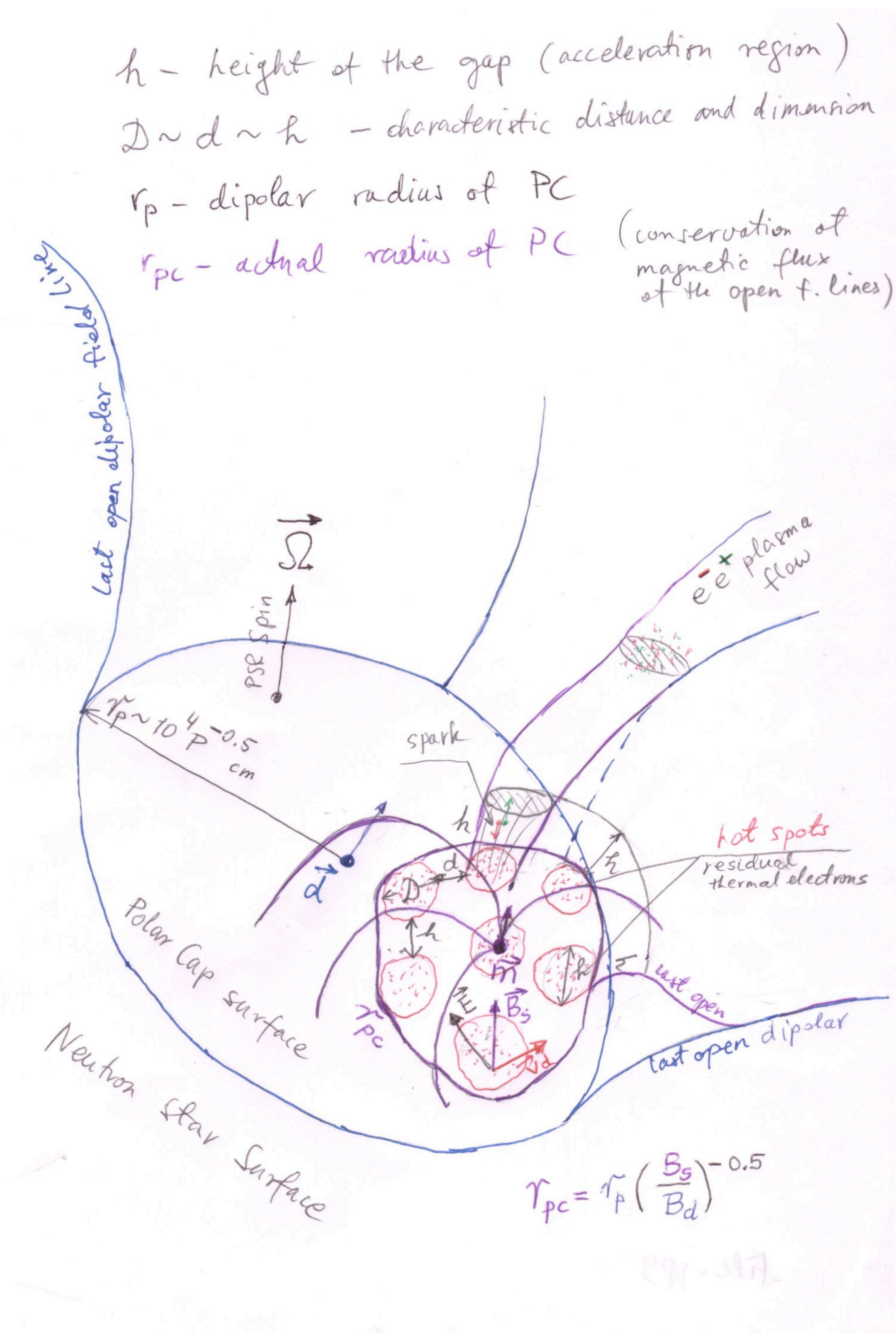

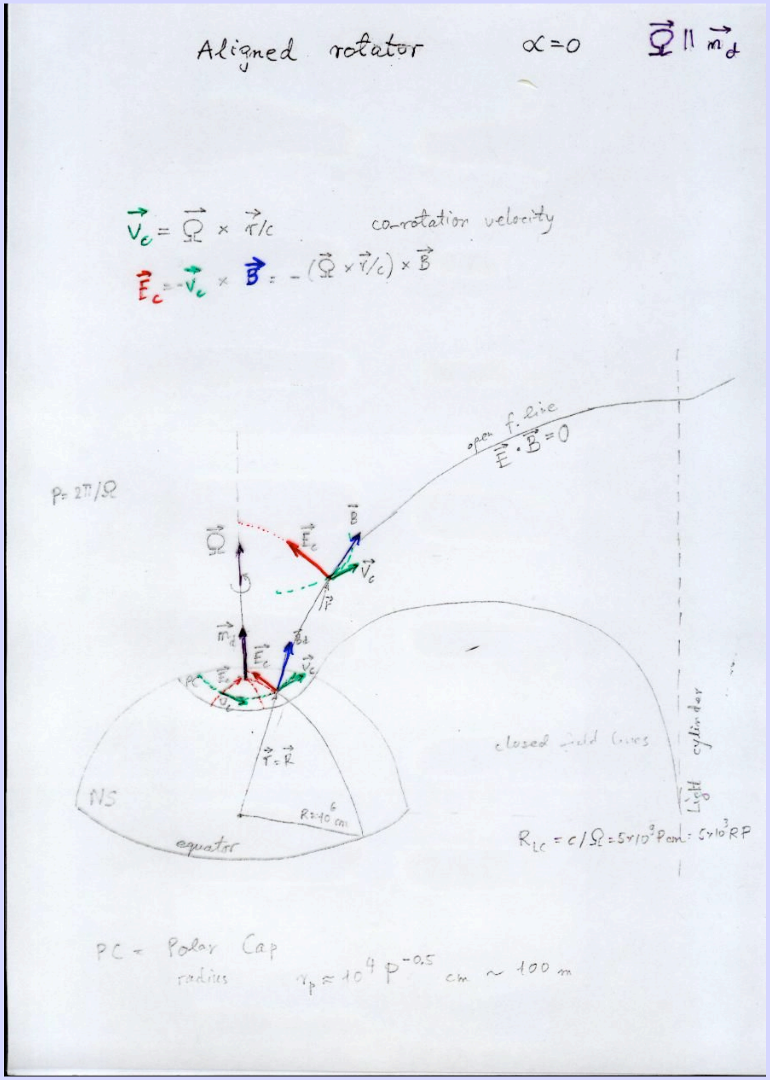
Aligned rotator α=0 Ω ∥ m_d
v_c = Ω × r/c co-rotation velocity
E_c = -v_c × B = -(Ω × r/c) × B
open f. line
E · B = 0
P = 2π/Ω
closed field lines
Light cylinder
NS
equator
r = R
R = 10^6 cm
R_LC = c/Ω = 5×10^9 P cm = 5×10^3 R P
PC = Polar Cap
radius r_p ≈ 10^4 P^-0.5 cm ~ 100 m

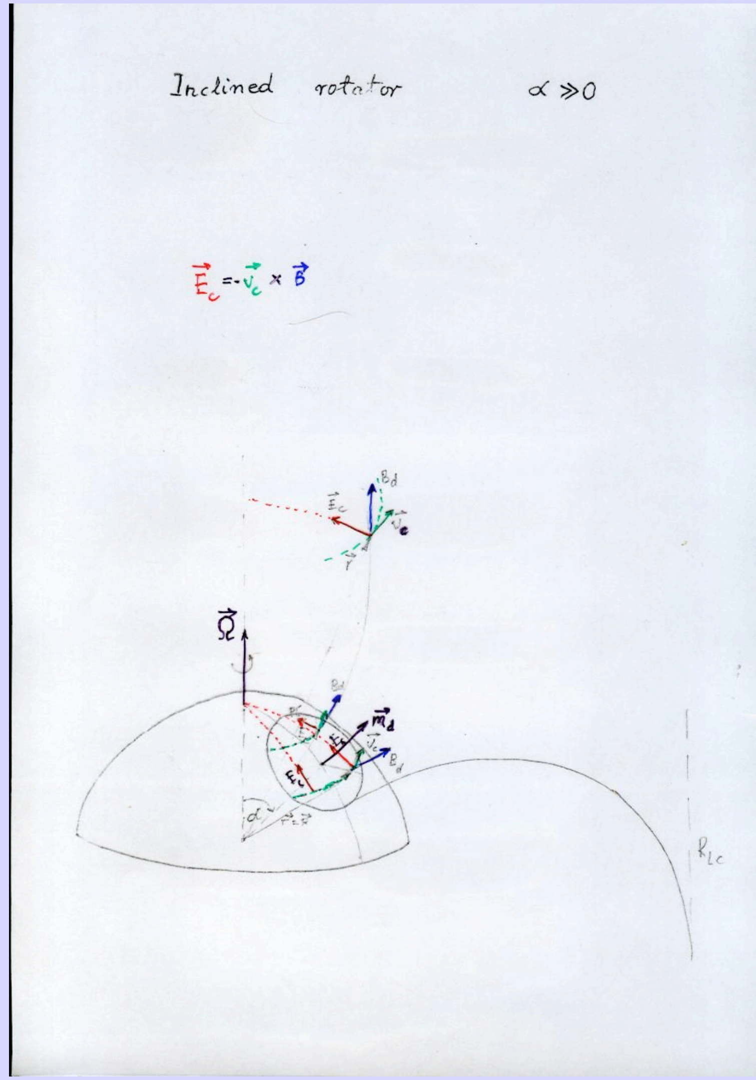
Inclined rotator α ≫ 0
E_c = -v_c × B
m_d
B_d
R_LC